

See discussions, stats, and author profiles for this publication at: <https://www.researchgate.net/publication/280028411>

Archean turbidite hosted orogenic gold mineralization in the Gadag greenstone belt, Western Dharwar Craton, Peninsular India

Article in *Ore Geology Reviews* · July 2015

DOI: 10.1016/j.oregeorev.2015.06.020

CITATIONS

9

READS

391

3 authors:



Ugarkar A. G.

Karnatak University, Dharwad

43 PUBLICATIONS 121 CITATIONS

[SEE PROFILE](#)



Murigeppa A Malapur

Karnatak University, Dharwad

8 PUBLICATIONS 17 CITATIONS

[SEE PROFILE](#)



Dr. Chandan Kumar B

Central University of Kerala

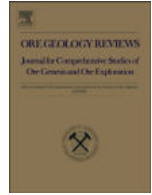
35 PUBLICATIONS 112 CITATIONS

[SEE PROFILE](#)

Some of the authors of this publication are also working on these related projects:



Precambrian Greenstone Belts: their genesis and role in crustal evolution [View project](#)



Archean turbidite hosted orogenic gold mineralization in the Gadag greenstone belt, Western Dharwar Craton, Peninsular India



A.G. Ugarkar *, M.A. Malapur, B. Chandan Kumar

Department of Studies in Geology, Karnatak University, Dharwad 580003, India

ARTICLE INFO

Article history:

Received 23 January 2015

Received in revised form 30 May 2015

Accepted 22 June 2015

Available online 3 July 2015

Keywords:

Dharwar Craton

Gadag greenstone belt

Turbidite-gold

Mineralogy

Geochemistry

Wallrock alteration

ABSTRACT

Turbidite hosted orogenic gold mineralization in the Archean Gadag greenstone belt of the Western Dharwar Craton, forms a major auriferous zone (Central Auriferous Zone) extending over a strike length of about 12 km in the Gadag duplex. The turbidite sequence comprises thick inter-bedded, medium to coarse grained lithic gray-wacke and thin laminated layers of fine grained carbonaceous phyllite. Gold bearing quartz veins impregnate preferentially along the en-echelon shear planes, fractures and schistosity planes. Auriferous quartz veins are enveloped by the altered wall rocks.

Mineralogy of the auriferous zone is dominated by gangue minerals like quartz, ankerite, chlorite, sericite and carbonaceous matter, with subordinate plagioclase. Monazite and xenotime are the important accessory minerals. Arsenopyrite and pyrite are the major sulfide minerals, but pyrrotite, chalcopyrite, sphalerite, galena and scheelite are also present. Gold in native state occurs within quartz, silicates and arsenopyrite.

Notable distinctions in mineral assemblage, texture and in chemical compositions of altered wall rocks compared to the precursor host rock in the study area implies that the metasomatism and wall rock alterations are the results of pervasive infiltration and intense interaction between hydrothermal fluids and the surrounding host rocks over a prolonged period.

Sulfides, carbonates, carbonaceous matter, K₂O, MgO, CaO, Cr, Ni, Cu, Pb, Zn, As and higher values of gold (0.98–4.72 ppm) are added into the altered wall rocks, immediately enveloping the auriferous quartz vein bodies. The chondrite normalized REE pattern of altered wall rocks exhibits enriched LREE (La_N/Yb_N = av. 9.54), with prominent negative Eu anomaly. The observed variation in geochemical characteristics and mineral assemblages in the alteration zones indicates differential response of the host rock and intensity of alteration depending on the composition of host rocks and hydrothermal fluids.

The auriferous hydrothermal fluids were of low salinity (2.0 to 6.6 wt.% NaCl), dominated by CO₂–H₂O (about 30 mol% CO₂) with moderate densities (0.7 to 1.04 g/cm³), and gold deposition occurred over a wide temperature range between 175 °C and 325 °C. Gold deposition was influenced by fluid mixing, phase separation and redox reactions. Mixing between CO₂–H₂O fluids and more reduced fluids, which evolved during fluid reaction with adjacent carbonaceous wall rocks, was the key factor causing gold deposition.

The formation of the Gadag duplex, deformation, folds and reverse strike slip faults (discontinuities) was caused by the compression associated with subduction related tectonic processes. During the initial period of intrusive magmatism (2,555 ± 6 Ma), regional metamorphism occurred in the entire greenstone belt, while during later period, hydrothermal fluids responsible for gold mineralization probably were derived from metamorphic processes as well as from intrusive granites. Such fluids channeled through the thrust in host turbidite sequence carrying dissolved gold, associated metals and sulfur, ultimately were precipitated in a reducing environment in the splays to the thrust in the Gadag duplex at about 2,522 ± 6 Ma, resulting in retrograde alteration assemblages.

© 2015 Elsevier B.V. All rights reserved.

1. Introduction

An improved understanding of gold deposits in metamorphic terrains, especially in the last three decades (Groves et al., 1998; Kerrich et al., 2000; Goldfarb et al., 2005; Large et al., 2011; Xue et al., 2013; Tomkins, 2014), has witnessed the comprehensive communication of

the distribution of epigenetic gold deposits in China as well as in Russia and in Asian countries (e.g. Kerrich, 1993; Ugarkar et al., 2000; Zhou et al., 2002; Mishra and Pal, 2008; Yakubchuk et al., 2002; Tomilenko et al., 2010; Sarma et al., 2011, and references therein). Thus, the distribution of gold in metamorphic terrains over geologic time has become fairly well established, as summarized by Kerrich et al. (2000), Goldfarb et al. (2005) and Groves et al. (2003). In recent years, systematic approach has been made in studying gold deposits, particularly to classify and in understanding their genetic aspects. As a result, three main classes of

* Corresponding author.

E-mail address: agugarkar@gmail.com (A.G. Ugarkar).

deposits are defined, each having a range of specific deposit types with common mineralogical, lithological, genetic and geodynamic settings, namely the orogenic (ORG), reduced intrusion-related (RIR) and oxidized intrusion-related (OIR) ones (Groves et al., 1998; Sillitoe and Thompson, 1998; Poulsen et al., 2000; Goldfarb et al., 2005; Robert et al., 2007). However, other types of globally important gold deposits include Carlin, Au-rich VMS and Witwatersrand type deposits (Sillitoe and Bonham, 1990; Huston, 2000; Hofstra and Cline, 2000; Law and Phillips, 2005).

The orogenic type of deposits constitutes a distinctive class of epigenetic precious metal deposits that are generated at mid-crustal levels (5–15 km) proximal to terrain boundaries, in transpressional subduction–accretion complexes of Cordilleran-style orogenic belts (Groves et al., 1998; Kerrich et al., 2000). Generation and transportation of hydrothermal fluids and deposition of gold from such fluids are attributed to these fundamental geological and tectonic processes. The specific deposits in this clan include the turbidite-hosted and greenstone (metavolcanic) hosted vein deposits, as well as the banded iron formation-hosted veins and sulfidic replacement deposits (Kerrich et al., 2000; Robert et al., 2007). As there remains some ambiguity in the distinction between ORG and RIR deposits, Goldfarb et al. (2005) and Robert et al. (2007) restrict the ORG to deposits composed of quartz–carbonate veins and associated wall rock replacements and their equivalents hosted in metamorphosed terrains associated with compressional or transpressional geological structures such as reverse faults and folds formed at mid-crustal levels. The auriferous zones are located on regional structures where there are large scale discontinuities with strike-slip duplexes (Sibson, 1990; McCuaig and Kerrich, 1998; Kerrich et al., 2000). So far, more than hundred gold deposits of this nature have been reported from different parts of the world (Goldfarb et al., 2005). Further, in orogenic deposits, three main types are distinguished based on their host-rock environment: greenstone-hosted (e.g. Dome; Norseman, Groves et al., 2003; Goldfarb et al., 2005), turbidite-hosted (e.g. Bendigo, Stawell, Victoria; Hodgson, 1993; Bierlein et al., 2000; Robert et al., 2005) and BIF-hosted (e.g. Homestake, Lupin; Caddey et al., 1991; Kerswill, 1996). Gold deposits hosted by turbidites have wide distribution throughout the world, occurring in rocks ranging in age from Archean to Tertiary; their abundance is less compared to greenstone hosted gold deposits. However, turbidite hosted terrains have been important sources of gold, particularly in Victoria of Australia, Nova Scotia, Canada, SE Guizhou, China (Kontak et al., 1990; Cox et al., 1995; Lu et al., 2005).

Three main types of orogenic gold deposits are present in various Neoproterozoic greenstone belts of Dharwar Craton of southern Peninsular India. They are metavolcanic-hosted deposits in Kolar, Hutti, Ramagiri and Mangalur belts, turbidite-hosted deposit of Gadag belt and BIF-hosted deposits of Kolar, Chitradurga and Gadag belts (Narayanaswamy and Ahmed, 1963; Rao and Reddy, 1985; Ugarkar and Tenginkai, 1988; Sawkar et al., 1995; Ugarkar and Deshpande, 1999). The Archean Gadag greenstone belt (Fig. 1) hosting gold mineralization in all the three types of host rocks, which is the subject of present paper, forms the most deserving example of orogenic type of gold mineralization. This is the only greenstone belt in the Dharwar Craton, where gold mineralization occurs in turbidite sequence, apart from metavolcanics and banded iron formations in a duplex structure (Gadag duplex). A complete study of characteristics of mineralization and geological anatomy of such a gold deposit is of fundamental importance for better understanding of the evolution of the greenstone belt and gold mineralization event. The present paper deals with the field, petrographic, mineralogical, geochemical and ore fluid characteristics of turbidite hosted Central Auriferous Zone and host rocks in understanding gold mineralization and prevailing geodynamics in the Gadag greenstone belt.

2. Regional geology

The Dharwar Craton, which includes several Archean greenstone belts, is one of the ideal terrains for understanding the nature of the

Archean crustal evolution and metallogeny. The craton has been divided into two distinct blocks, the Western Dharwar Craton (WDC) and the Eastern Dharwar Craton (EDC) based on the nature and abundance of greenstones, crustal thickness, grade of regional metamorphism and degree of melting (Swami Nath et al., 1976; Rollinson et al., 1981; Jayananda et al., 2006; Chardon et al., 2011). The steep mylonitic zone, a major thrust-fault contact (Chitradurga Thrust Fault) along the eastern margin of the Chitradurga greenstone belt, extending over a length of 400 km from Gadag in the north to Mandya in the south is considered as the boundary between the two blocks (Kaila et al., 1979; Chadwick et al., 2000; Sengupta and Roy, 2012). The volcano–sedimentary association present in the greenstone terrains of the WDC and EDC displays distinct geodynamic settings, as deciphered by recent petrological and geochemical studies (Balakrishnan et al., 1999; Manikyamba et al., 2008, 2014; Manikyamba and Kerrich, 2011; Jayananda et al., 2013, 2014; Ugarkar and Nyamati, 2002; Ugarkar et al., 2000, 2013). Based on combined U–Pb zircon ages and Nd isotope data, the craton has been divided into three provinces western (3.4 to 3.2 Ga), eastern (3.4 to 3.2 Ga) and central with mixed old and younger crust (3.4 to 3.2 Ga and 2.56 to 2.52 Ga) and eastern with mainly younger (2.56 to 2.52 Ga) crust (Peucat et al., 2013; Jayananda et al., 2013). However, the western and eastern greenstone terrains record different geological, geophysical and structural characteristics (Manikyamba et al., 2014; Borah et al., 2014). The WDC is dominated by old basement (>3.2 Ga TTG with interlayered Sargur Group greenstone belts) which is unconformably overlain by 2.9 to 2.7 Ga Dharwar Supergroup volcano–sedimentary greenstone belts (Swami Nath and Ramakrishnan, 1981; Nutman et al., 1996; Peucat et al., 1993; Jayananda et al., 2008, 2012; Sarma et al., 2011). The Dharwar Supergroup is divided into a lower Bababudan Group and an upper Chitradurga Group (Swami Nath and Ramakrishnan, 1981). The EDC comprises younger (2.7 to 2.6 Ga) gray tonalitic gneisses with large remnants of 3.0 to 3.32 Ga TTG (Krogstad et al., 1991; Peucat et al., 1993; Balakrishnan et al., 1999; Jayananda et al., 2000; Chardon et al., 2002), thin elongated 2.7 to 2.56 Ga volcanic dominated gold bearing greenstone belts of Kolar Group and diamondiferous kimberlites (Swami Nath et al., 1976; Balakrishnan et al., 1990, 1999; Jayananda et al., 2012). The whole Archean crust in the Dharwar Craton was affected by at least four major tectonothermal events at 3.24 Ga, 3.1–3.0 Ga, 2.62 Ga and 2.51–2.45 Ga (Peucat et al., 1993, 2013; Jayananda et al., 2011, 2013; Chalapatih Rao et al., 2013). The craton corresponds a large tilted oblique section of the Archean continental crust, and from north to south in the craton, in general, there is a progressive increase in the grade of metamorphism from greenschist facies to granulite facies.

In the WDC, the Sargur Group greenstone sequences are dominated by 3.35 Ga komatiite–basalt metavolcanic sequences with interlayered sediments corresponding to shelf environment (Naqvi and Rogers, 1987; Jayananda et al., 2008). The lithounits comprise banded iron formations, fuchsite quartzite of detrital origin, metapelites, basaltic amphibolites, metaperidotites, and stratiform gabbro anorthosites (Radhakrishna and Vaidyanathan, 1997). Metamorphic grade in the Sargur is amphibolite facies grading into granulite facies (Swami Nath and Ramakrishnan, 1981). Chromite, barite, magnesite, titaniferous magnetite, nickel, platinum and copper mineralization occur in the Sargur Group (Radhakrishna and Vaidyanathan, 1997; Devaraju et al., 2009). The Bababudan Group comprises mafic–ultramafic volcanics, arenites, phyllites, polymict and oligomictic conglomerates and banded iron formations (Swami Nath and Ramakrishnan, 1981; Naqvi and Rogers, 1987). Thin lenses of carbonate rocks are, however, seen with iron formations. Manganese formation is conspicuously absent in this group. The metamorphism is mainly amphibolite facies at the borders of the belts with greenschist facies at the portions. The Chitradurga Group comprises mafic–ultramafic volcanic rocks, banded iron formations, arenites, phyllites, stromatolitic carbonates, carbonaceous phyllites, polymict and oligomictic conglomerates, graywackes and felsic metavolcanics (Swami Nath and Ramakrishnan, 1981). The

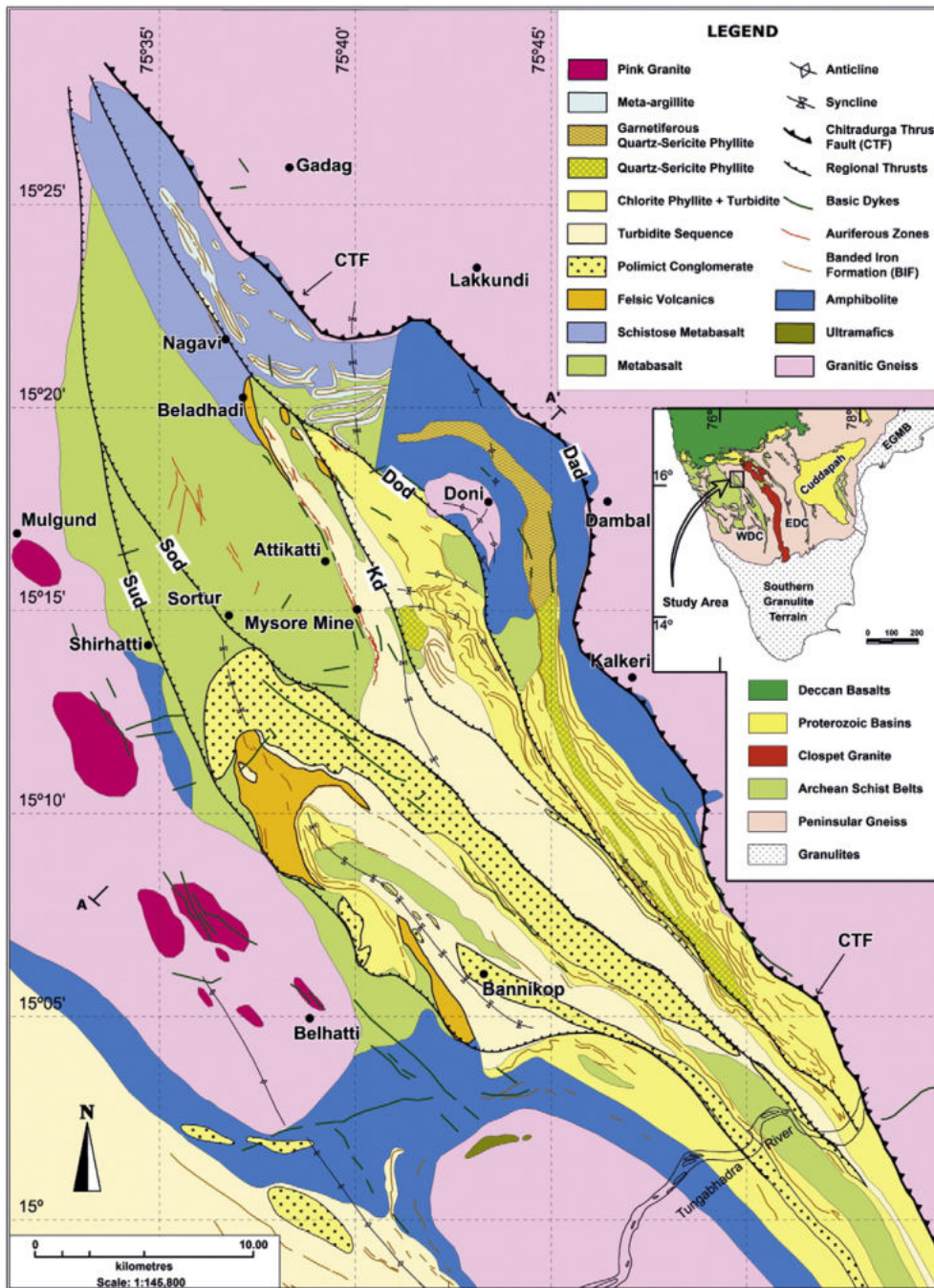


Fig. 1. Geological map of the Gadag greenstone belt. Modified after Ramachandran et al. (2001).

sedimentary iron and manganese ores constitute the significant association of this group. Copper, gold, lead and zinc mineralization also occur and the greenschist facies metamorphism is extensively developed in this group (Naqvi and Rogers, 1987).

The greenstone belts of the Dharwar Craton host a number of orogenic type gold prospects and a few deposits of mining scale like Kolar, Hutti, Hira-Budhini, Ramagiri and Mangalur deposits in EDC and Bellara, Ajjanahalli, and Gadag deposits in WDC (Vasudev et al., 1994; Radhakrishna and Curtis, 1999). Within the greenstone belts of EDC, more than 120 ancient old workings for gold have been recorded. In the WDC, the crustal scale shear zone along the Gadag–Chitradurga greenstone belt represents an auriferous shear zone system with more than 26 old workings apart from above-mentioned deposits.

3. Geology of Gadag greenstone belt

The Gadag greenstone belt is considered to be the northern continuation of the Chitradurga greenstone belt due to the continuity in lithological associations and structural coherence (Naqvi and Rogers, 1987). It comprises older Peninsular Gneisses, metavolcanic and metasedimentary rocks, K-rich granites and younger intrusives (Ugarkar and Deshpande, 1999; Ram Mohan et al., 2014). The metavolcanic suite of rocks belongs to the Ingaldhal Formation that is conformably overlain by metasedimentary sequence belonging to the Hiriyr Formation of the Chitradurga Group. The metavolcanics represent a mafic–intermediate–felsic suite comprising basalt, basaltic andesite, andesite, dacite and rhyolite, while the metasediments consist

of polymict conglomerate, graywacke, chlorite phyllite, quartz-mica schist, garnetiferous quartz-mica schist, banded iron formation, and minor bands of carbonates (Ugarkar and Deshpande, 1999). The volcanic and sedimentary sequences developed schistosity due to the formation of platy minerals like chlorite, sericite, muscovite and biotite, and also their disposition along the limbs of the folds. The grade of metamorphism varies from greenschist in the center to lower amphibolite facies at the periphery. Mafic metavolcanics are low K, Fe-rich tholeiites derived by partial melting of the upper mantle source, while the intermediate and felsic metavolcanics were derived by re-melting of these tholeiites mainly in the crustal regimes (Ugarkar et al., 2000). Clastic metasediments had a sialic dominated mixed felsic and mafic source in the provenance (Ugarkar and Nyamati, 2002). The U–Pb zircon ages for felsic metavolcanics from the central part of the Gadag greenstone belt indicate volcanism at 2588 ± 10 Ma (Sarma et al., 2011). While a U–Pb SHRIMP zircon study of turbidite graywackes from the GGB constrains the maximum sedimentation age from the youngest detrital population as 2547 ± 5 Ma (Sarma et al., 2012). These volcano-sedimentary rocks had different tectonic settings of subduction complex and they occur juxtaposed, probably by accretion process during convergence of plate (Ugarkar et al., 2000; Ugarkar and Nyamati, 2002).

The granites on either side of the belt are granites and granodiorites, which show diffused magmatic banding and are variably mylonitized. Geochronological data indicates about 2.56 Ga granitic magmatism surrounding this belt in the WDC, which was derived from intracrustal melting of an arc resembling crust, without the involvement of mantle, and demonstrates the prevalence of horizontal tectonics in the evolution of the Dharwar Craton (Ram Mohan et al., 2014). Based on bouguer gravity anomalies, it is suggested that the Gadag belt is bounded on either side by faults (F_1 and F_2), and that essentially represents the contacts between supracrustal rocks and younger granites (Ramadass et al., 2003). A tectonized intrusive relationship has been established between the eastern margin granitic rocks and the eastern margin of the belt. Shallow linear fabrics and sinistral displacement are consistent all along the eastern margin of the belt, suggesting that these granitic rocks are most likely part of the Dharwar Batholith (Chadwick et al., 2000), which is confirmed by regional studies along eastern margin of the belt, defining the Gadag–Mandya shear zone (Sengupta and Roy, 2012). Two major deformation events have been suggested based on the regional structural studies, where the first deformation event (D_1) resulted in NW–SE trending pervasive fabrics and schistosity (S_1), and the second deformation event (D_2) defines the general NNW–SSE tectonic trend that marks the regional disposition of the belt (Ramachandran et al., 2001; Chadwick et al., 2003; Sengupta and Roy, 2012). A weaker third deformation event (D_3), with E–W or ENE–WSW axial traces recorded locally (Beeraiyah et al., 2001).

The regional structure as described by Narayanaswamy and Ahmed (1963) is an asymmetrical isocline with axial plane dipping to the east. In the widest part Gadag belt, the lithological assemblage is ~17 km thick (perpendicular to dip), and thickness is the result of overturning on large scale folds and stacking on reverse faults (Chadwick et al., 2003). Based on the reconnaissance mapping, satellite imagery and structural studies, Chadwick et al. (2003) proposed that the rocks are components of a hinterland-dipping duplex that was termed as the “Gadag duplex”, which comprises four thrust slices (Doni, Doni Tanda, Attikatti and Majjur domains), that are separated by reverse faults labeled, from NE to SW, the Dambal, Doni, Keluru, Sortur and Suganhalli discontinuities. The duplex is underlain by the Vadvi domain that forms the part of the Chitradurga greenstone belt. The plutonic rocks (Srimant Gudda and Hebbal domains) and the Vadvi domain form the foot wall block of the duplex, while the hanging wall block tectonically overlying the duplex is represented by mylonite granites (Lakkundi domain). The orientation of the rocks throughout the GGB is NW–SE to NNW–SSE, with a strong tectonic fabric dipping east to a moderate angle.

4. Gadag gold field

4.1. Historical background

Gold mineralization in Gadag greenstone belt is spatially distributed in distinct clusters and linear groups along shear zones, and the entire area covering about 120 km² is popularly known as the Gadag Gold Field (Fig. 2). A detailed account of the historical mining activity and potentiality of individual auriferous reef systems has been given by Curtis and Radhakrishna (1993). The Gadag Gold Field was known for extensive gold mining activity in ancient time which lasted from about four thousand years before present, to about 500–600 A.D. when all mining activities were ceased. Mining activities were resumed in 1902 and lasted less than decade. Maclaren (1906) was the earliest to give the geological account on the deposition of gold bearing reefs. To investigate the extension of gold mineralization and its possible economic viability, the Hutti Gold Mines, Bharat Gold Mines, Geological Survey of India, Mineral Exploration Corporation Limited and Mineral Sales Private Limited have carried out extensive exploration in the Gadag Gold Field, and it has been emphasized that this gold field holds mining potential and mines could be developed to produce the yellow metal (Curtis and Radhakrishna, 1993; Sawkar et al., 1999).

4.2. Auriferous zones

The Gadag Gold Field includes three auriferous zones namely, Western, Central and Eastern auriferous zones, each with a distinct lithological assemblage, occur within the shear zones of metavolcanics and metasediments, and they are almost parallel to the regional trend of the schistosity (Narayanaswamy and Ahmed, 1963; Ugarkar and Deshpande, 1999). A cross section across the Gadag gold field indicates that these auriferous zones are restricted to the Gadag duplex (Fig. 3) of Chadwick et al. (2003).

The Western Auriferous Zone (WAZ) is hosted by pillowed metabasalt and andesite underlying the turbidites in the Attikatti domain. This system lies along a linear zone just east of Hosur parallel to the regional strike of the schistosity. This system extends over 2 km, and the gold value ranges between 0.3 and 19 g/t, with an average grade of 4.02 g/t.

The Central Auriferous Zone (CAZ), the main auriferous zone, occurs in the Attikatti domain, at the sheared lithological contact of metavolcanic and metasedimentary rocks. However, mineralization is more significant in the turbidite sequence of rocks. The extension of auriferous zone is parallel to the fold axial trace of the Kadakol syncline plunging southeast. This zone extends over a strike length of about 12 km. The gold content ranges between 0.42 and 20 g/t, with an average grade of 4.77 g/t.

The Eastern Auriferous Zone (EAZ), a less persistent zone, is hosted mainly by banded iron formation and phyllites of the Doni domain. Gold content ranges between 0.27 and 9.6 g/t, with an average grade of 2 g/t.

Parallelism between the linear strike-parallel distribution of auriferous zones, the axial trace of the anticline in the western zone and syncline in the central zone and the regional cleavages/schistosity points to a close relationship between the movement and focusing of gold bearing hydrothermal fluids, folding and cleavages/schistosity. The Gadag duplex as termed by Chadwick et al. (2003) comprises of domains that are separated by over stacking discontinuities (thrusts), which might have acted as splays. Such splays having interlinked with large scale thrusts, might have acted as fluid paths leading to the precipitation of gold in sub-parallel to en-echelon splays of secondary or tertiary order as observed in gold deposits elsewhere (Kerrich et al., 2000; Goldfarb et al., 2005).

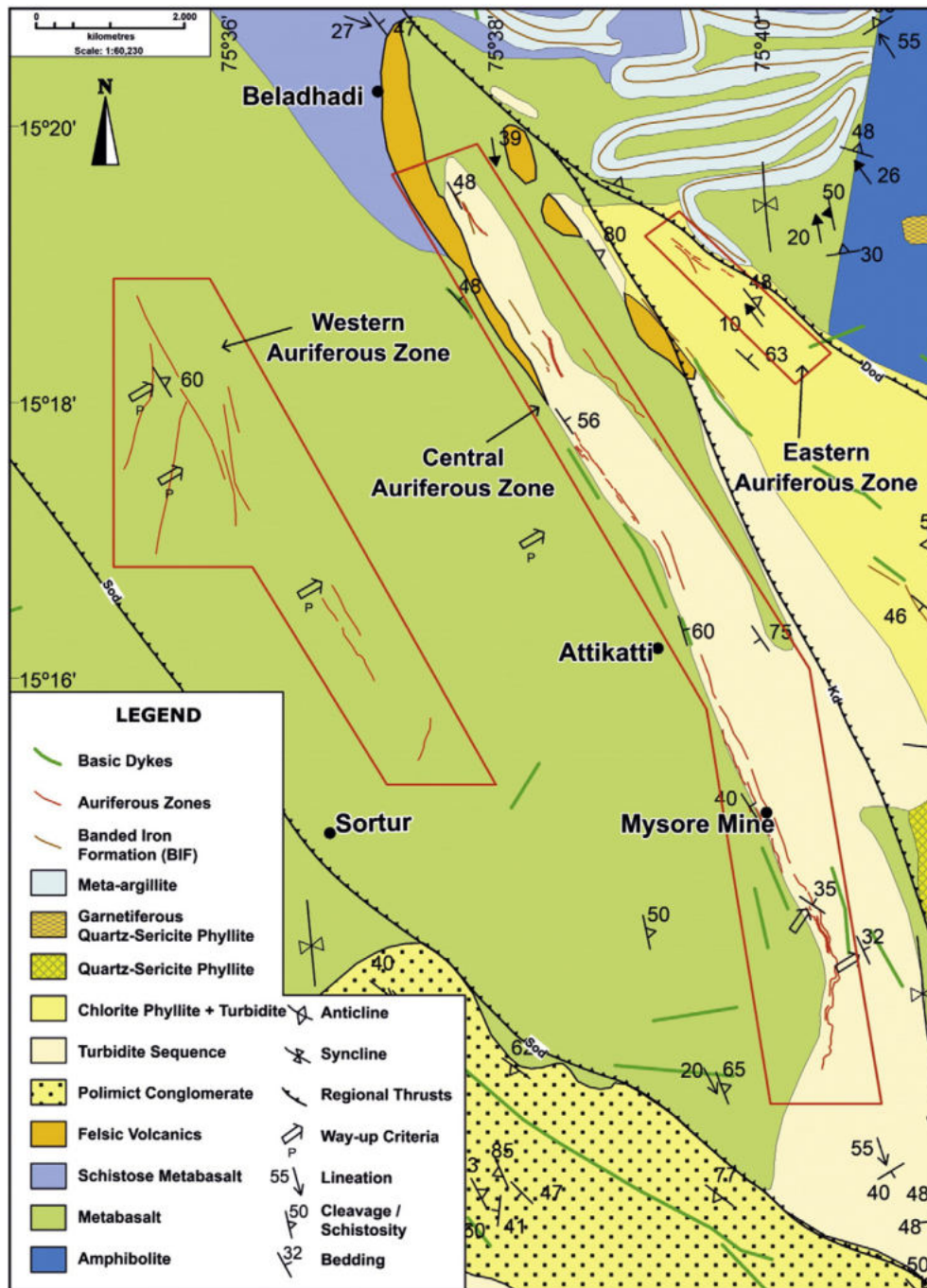


Fig. 2. Geological map of the Gadag gold field showing Western, Central and Eastern Auriferous Zones.

5. Petrography of host turbidites

Turbidite sequence of Gadag greenstone belt that hosts the Central Auriferous Zone comprises interbedded sequence of thick, medium to coarse grained graywacke and thin laminated layers of fine grained carbonaceous phyllite. Graywackes are greenish gray, fine to coarse grained and exhibit clastic texture with angular, sub-angular to sub-rounded clasts. Modal analysis shows that the graywackes consist of clasts of quartz (21%), rock fragments (6% volcanic, 23% chert + quartzite) and feldspar (3% K-feldspar, 8% plagioclase) embedded in a matrix of chlorite + sericite (33%) and calcareous material (6%). Both mafic and felsic volcanic rock fragments are observed among the volcanic fragments and quartz is of mono- and polycrystalline types, and is found in equal

abundance. Plagioclase is more abundant than K-feldspar and the ratio between them (plagioclase/K-feldspar) is greater than 1 (av. 2.2). Andesine is the most common plagioclase found in these samples. Due to metamorphism and deformation, the rock exhibits schistosity, and the matrix minerals show orientation along schistosity planes. The matrix includes recrystallized fine-grained quartz, mica, feldspar, iron oxides and clay minerals. When plotted in QFL diagram (figure not shown) of sandstone classification, these graywackes fall in the class of lithic wackes. Carbonaceous phyllite is dark gray to black, fine grained schistose rock. Compositionally it is almost similar to chlorite phyllite. In addition to chlorite, sericite, quartz and carbonates, it has carbonaceous matter. Very fine carbonaceous matter occurs as thin line along schistosity planes and tends to bend around quartz and other minerals present in the rock.

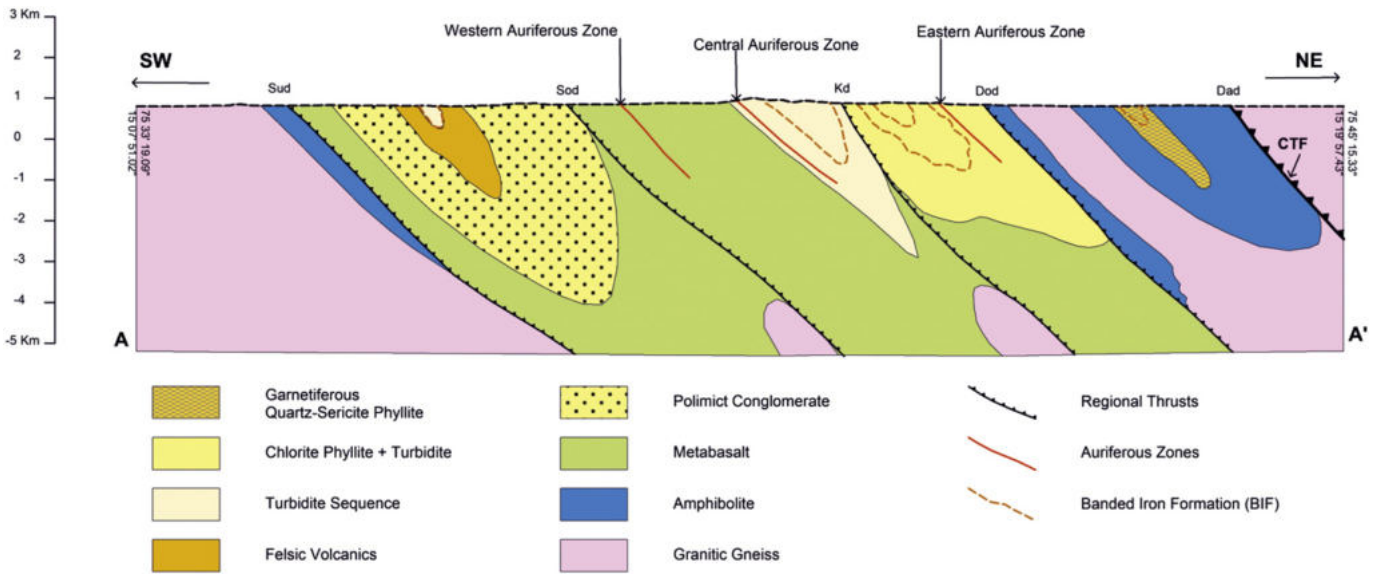


Fig. 3. SW–NE cross section across the Gadag duplex showing disposition of auriferous zones of Gadag greenstone belt. Section line on the geological map of Gadag belt is along A–A' (Fig. 1).

Because of its opacity and black color, the carbonaceous matter appears more prominent.

6. Turbidite hosted gold mineralization and hydrothermal alterations

In the Central Auriferous Zone, which is hosted mainly in the turbidites, two types of gold bearing quartz veins impregnate preferentially along the en-echelon shear planes, fractures and schistosity planes. The main auriferous quartz veins are of about 15 cm to 1.50 m thick milky white and at places they contain extensive patches of chlorite, sericite and carbonaceous matter (Fig. 4a). They also show rusty brown encrustations left after the secondary surface alterations of ankerite and pyrite grains (Fig. 4b). The other types of auriferous quartz veins are of ~15 cm thick, bluish dark gray in color. They display distinct fine banding parallel to vein walls and schistosity of host rock (Fig. 4c). These bands contain carbonaceous matter and tiny grains of sulfides. These veins are cut across by secondary veins of sulfides and quartz (Fig. 4d). These features suggest probable episodic hydrothermal activity.

Turbidite hosted hydrothermal gold deposits, such as those found in Victoria, SE Australia, lack significant wall rock alterations and diagnostic alteration haloes (Bierlein et al., 2000). The visible wall rock alteration in turbidites may often be weakly developed because the host rock composition did not allow extensive development of distinct alteration assemblages, such as those recognized in reactive mafic host volcanic rocks of Archean lode gold deposits. However, the Central Auriferous Zone of Gadag belt is characterized by hydrothermal wall-rock alterations represented by chloritization, sericitization, carbonatization, silicification, and sulfidation with ubiquitous presence of carbonaceous matter. One of the most significant features of wall rock alteration is marked bleaching of the host rock due to abundant sericite, carbonates, as well as the development of large disseminated porphyroblasts of arsenopyrite (Fig. 4e), pyrite and carbonate spots. Sulfides are best developed within a few meters (~4 m) of the main auriferous quartz vein. Euhedral arsenopyrites occur closest to the main reefs, whereas prophyroblasts of cubic pyrite can extend farther. At places, carbonaceous matter occurs as thin layers along schistosity planes and contains large granular grains of pyrite (Fig. 4f). Carbonaceous slickenside coatings and mobilization of carbonaceous matter between individual clastic frame work sand grains of graywacke (Fig. 5a) suggest a weak foliation. It also occurs as co-folded tiny veins with quartz veins (Fig. 5b)

in the altered wall rocks. All these features indicate mobilization of carbonaceous matter in the auriferous zones. As discussed above, in the study area, distinct development and demarcation of visible alteration haloes around auriferous quartz veins within host turbidite are difficult due to siliclastic nature of the host rock. The mineralogical and geochemical distinctions between different alteration types are sometimes difficult since more than one type may be present in a sampled area, consequently, the mineral assemblage and chemical analysis of the bulk rock often reflect the mixing of different alteration types. Due to such reasons, for present study of mineralogy and geochemistry of wall rock alterations, two preferably distinct types of alteration representing, silicified–carbonatized + sericitized rock (SCS) and chloritized–sericitized ± carbonatized rock (CSC) enveloping the gold quartz veins have been selected.

7. Sampling and analytical techniques

For the present study, the least altered host turbidite sequence samples were collected away from the shear zones, which were devoid of hydrothermal alterations, sulfides and veins of quartz and carbonates. Samples of wall rock alterations and ore vein quartz for whole rock analysis and mineral analysis were selected from the underground cuttings and bore holes of Mysore mine area of the Central Auriferous Zone.

Samples were powdered to ~200# manually in an agate mortar after preparing rock granules in a hand operated steel mortar. Geochemical analyses of these samples were carried out at the Geochemistry Laboratory of the National Geophysical Research Institute (NGRI), Hyderabad. Major oxides were analyzed by XRF whereas rare earth elements (REEs) were analyzed by ICP-MS (Perkin Elmer SCIEX ELAN DRC II). The analysis has been carried out using international standards GSR-4, GSR-5 and JG-1. The analytical procedures are referred to Balaram et al. (1996) and Gnaneshwar Rao and Govil (1995). Gold contents in the samples of auriferous zones were analyzed with FAAS (Varian SPECTRA A220) by methyl isobutyl ketone (MIBK) method following the procedure of Ramesh et al. (2001). The international standard reference samples used with certified values for gold were GAu-8 (0.5 ± 0.1 ppm), GAu-10 (5.3 ± 0.2 ppm), GAu-16 (1.09 ± 0.03 ppm) and GAu-18 (10.0 ± 0.2 ppm).

The samples for mineral analysis were collected from drilled cores and walls of old workings of the central and eastern auriferous zones. Mineral analysis has been carried out at the Institute of Electron Optics,

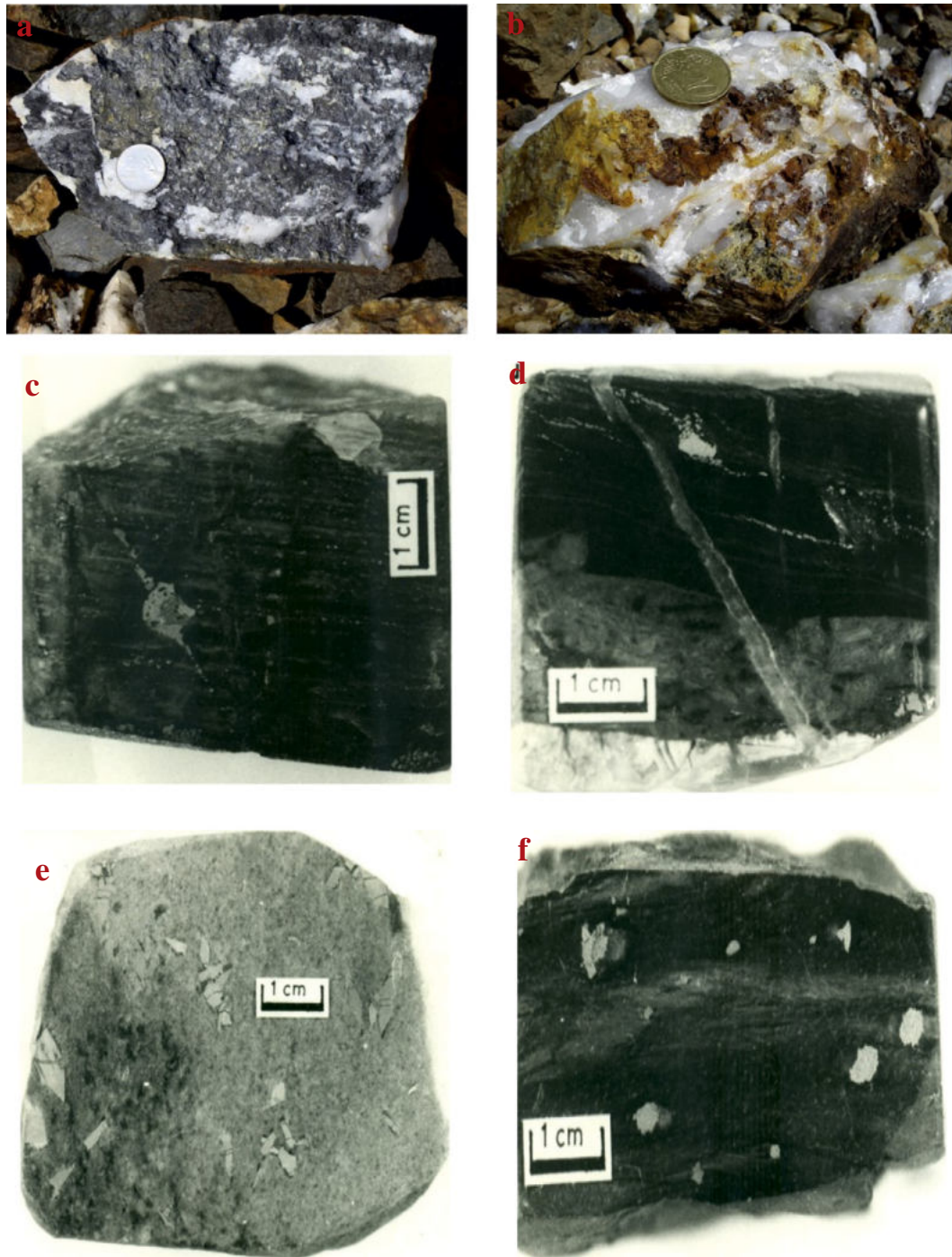


Fig. 4. (a) Auriferous milky white vein quartz from underground mine face, containing patches of chlorite, sericite and carbonaceous matter. (b) Auriferous milky white vein quartz from underground mine face containing showing rusty brown encrustations left after secondary surface alterations of sulfides and ankerite. Photographs of drilled cores: (c) and (d) Auriferous bluish dark gray vein quartz displaying fine banding parallel to vein wall, due to microbands of sulfides and carbonaceous matter. These veins are cut across by secondary veins of sulfides and quartz. (e) Disseminated large euhedral porphyroblasts of arsenopyrite in the altered wall rock of host. (f) Granular coarse grains of pyrite in finely laminated carbonaceous phyllite.

University of Oulu, Linnanmaa, Finland, employing JEOL-SEM equipped with an Energy Dispersive Spectrometer and LINK AN 10,000 X-ray analyzer, mainly following the method described by Alapieti and Sivonen (1983). Standard analytical conditions included an acceleration voltage of 15 kV and sample current of 1.5 nA. The standards used were wollastonite for Si and Ca, apatite for P and pure metals for the remaining elements. The practical detection limits varied from 0.05 to 0.5 wt.%, depending upon the element analyzed. ZAF-4 program has been adopted to make necessary corrections for overlapping peak of different elements. The analytical facilities of the labs are proved to be adequate

for obtaining acceptable analyses of grains measuring more than 1.5 μm . Microprobe analyses of selected minerals of the auriferous zone have been carried out.

8. Mineralogy of Central Auriferous Zone

The individual gangue minerals as well as ore minerals of the gold quartz veins and enveloped wall rocks of the Central Auriferous Zone are described below, along with the mineral chemistry of a few selected minerals (Table 1).

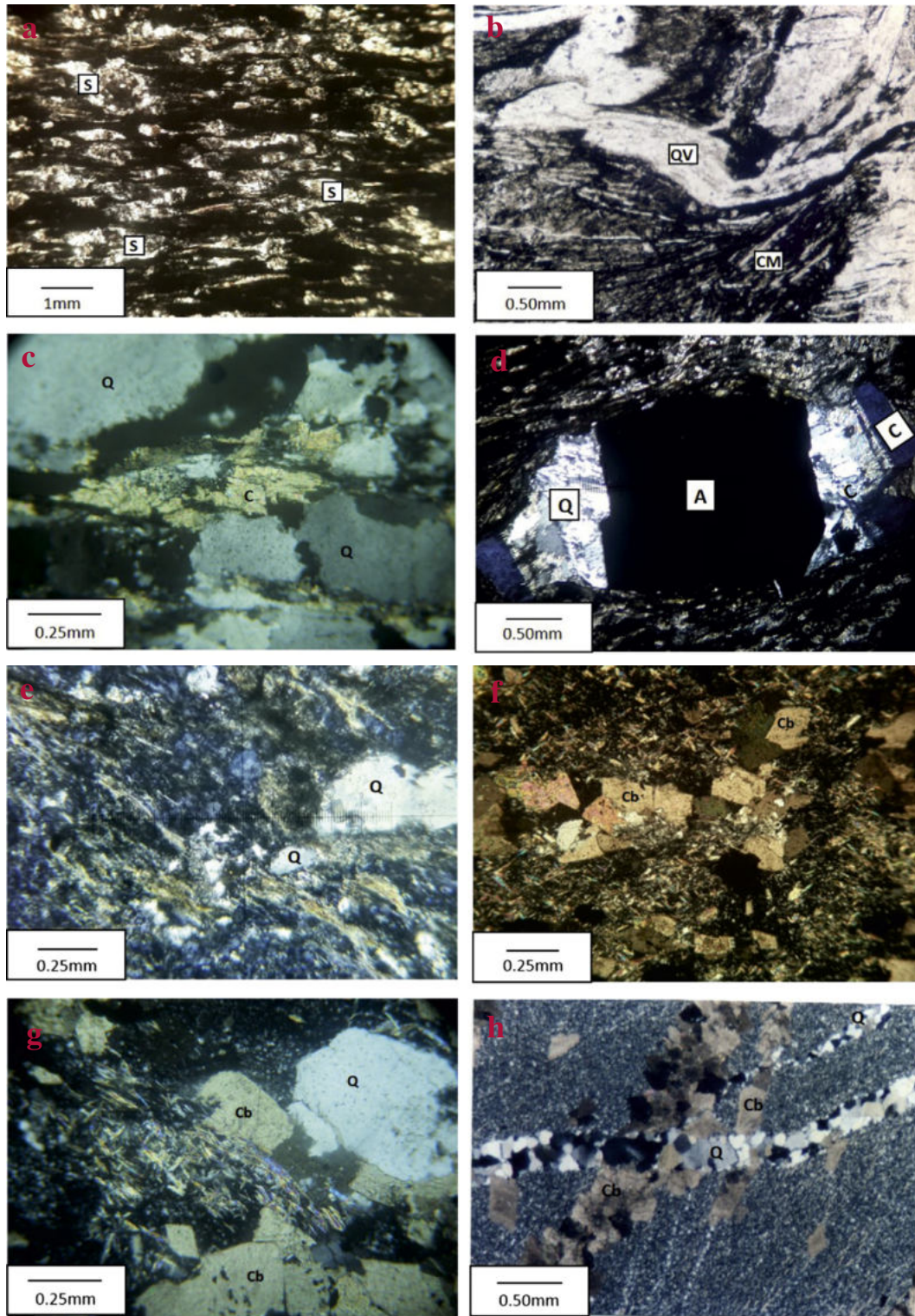


Fig. 5. Photomicrographs (transmitted light) of gangue minerals of auriferous zones: (a) Carbonaceous matter (black) occupying space between individual clastic sand grains (S) of turbidite graywacke in the alteration zone. Note the elongation and orientation of sand grains due to deformation and metamorphism. (b) Co-folded carbonaceous matter (CM) and quartz (QV) during deformation, indicating mobilization of silica and carbonaceous matter in the auriferous zone. (c) Quartz clasts (Q) of turbidite graywacke exhibiting sutured grain boundaries due to deformation and metamorphic effects, carbonates (C) occupy the spaces between the displaced sand grains. (d) Fibrous quartz (Q) fringes along with chlorite (C) develop perpendicularly to crystal faces of arsenopyrite (A). Note that chlorite growth abuts at framework grains within the host rock due to lack of space for its development. (e) Flakes and laths of chlorite (blue) and sericite (golden yellow) exhibiting foliation and alignment in the altered wall rock. Chlorite exhibits an anomalous blue interference color of chlorite, indicating penninite variety. Note the distorted sand grains (Q) of host rock. (f) Fine dispersed flakes of sericite and chlorite associated with subhedral to euhedral carbonates (Cb). (g) Development of sericite and chlorite (flakes) by alteration of lithic fragments and matrix between carbonates (Cb) and clasts of quartz (Q). (h) Tiny veins of carbonates (Cb) and quartz (Q) of late generation in the altered rocks.

Table 1
EPMA data of selected minerals of auriferous zone.

Monazite					
Wt.%	1	2	3	4	5
La ₂ O ₃	10.68	12.77	14.08	14.6	7.63
Ce ₂ O ₃	32.02	32.76	34.1	34.1	29.3
Pr ₂ O ₃	–	–	3.45	3.56	3.87
Nd ₂ O ₃	14.15	14.67	14.46	13.73	19.69
Y ₂ O ₃	6.67	5.59	–	–	–
ThO ₂	1.78	3.3	–	–	3.02
CaO	0.69	0.71	–	–	–
P ₂ O ₅	34	33.89	36.38	35.83	34.9
Total	99.99	103.7	102.47	101.82	98.41

Xenotime			Ankerite		
Wt.%	1	2	Wt.%	1	2
Y	51.82	53.26	FeO	17.947	17.795
P	15.64	15.34	MnO	1.421	1.516
O	34.23	34.19	MgO	7.45	7.78
CaO		25.878		25.594	

Arsenopyrite		
Wt.%	1	2
As	42.91	43.22
Fe	34.88	34.7
S	21.11	21.4
Au	0.23	0.34
Total	99.13	99.66

8.1. Gangue minerals

Quartz, apart from its occurrence as main auriferous quartz veins of varying dimensions as described in the previous section, constitutes the most common gangue mineral, especially as clasts in the altered turbidite wall rocks. Microscopic examination of quartz veins reveals the presence of chlorite, sericite, carbonates, carbonaceous matter and disseminated sulfides. Silicification is more pronounced and found to be an essential wall-rock alteration immediately surrounding the gold bearing quartz veins. Vein textures exhibit features of ductile deformation, like quartz mylonites in the form of elongate, stretched and strained quartz grains with sutured margins or ribbons in veins as well as in foliated wall-rocks. Quartz clasts of graywacke exhibit sutured grain boundaries due to deformation and metamorphic effects (Fig. 5c). Often fibrous quartz fringes along with chlorite develop perpendicularly to crystal faces of arsenopyrite (Fig. 5d).

Plagioclase is commonly seen in wall-rocks than in vein quartz. It occurs in the form of anhedral to subhedral clasts, and is altered to sericite. It also forms groundmass or matrix in wall-rocks. In the form of subhedral plates, it occurs together with carbonates. In such instances, the replacement of plagioclase by carbonate is a common feature.

Chlorite is an important mineral in these auriferous zones. It invariably exhibits an anomalous blue interference color, indicating penninite variety of chlorite (Fig. 5e). Chlorite flakes are commonly associated with sericite, carbonate and sulfide minerals. At places, along with quartz, it fringes away from the crystal faces of arsenopyrite (Fig. 5d), sometimes chlorite growth abuts at frame work grains within host rock due to the lack of space for its development. Chlorite also forms one of the components of ground mass or matrix of host rock.

Sericite, like chlorite, also forms an important mineral of altered wall-rocks. It occurs as fine dispersed flakes, laths and shreds, and is commonly associated with chlorite and carbonates (Fig. 5f). It also forms the matrix material of host turbidite graywackes. It is found in more abundance in wall rocks immediately close to auriferous quartz veins. Development of chlorite is a common feature in the wall rocks due to the alteration of lithic fragments and matrix material (Fig. 5g), resulting into the alignment of sericite laths and flakes along schistosity as well as shear planes and quartz mylonites.

Carbonate is an extensively occurring mineral in altered wall rocks and quartz veins. It occurs as subhedral to euhedral crystals oriented along schistosity of the host rock (Fig. 5f). It may be noted that the carbonaceous matter and the carbonates occur in significant quantity in the auriferous ore zones. Tiny veins of carbonates and quartz of late generation (Fig. 5h) are frequently noticed in the altered rocks. Many times, carbonates occupy the spaces between the displaced sand grains (Fig. 5c). Electron microprobe data of analyzed grains of carbonates indicate ankerite composition with MgO (7.45–7.78%), CaO (25.59–25.88%), FeO (17.79–17.95%) and MnO (1.42–1.52%).

Monazite and xenotime, in the form of irregular to euhedral tiny specks of 10–50 µm, occur as accessory minerals in association with quartz, carbonates, chlorite, sericite, sulfides and carbonaceous matter in the altered wall-rocks. At places, they occur as tiny inclusions in arsenopyrite, pyrite and silicates of wall rocks. Monazite mainly contains LREE i.e., La₂O₃ (7.63–14.60%), Ce₂O₃ (29.30–34.10%) and Nd₂O₃ (13.73–19.69%) and P₂O₅ (33.89–36.38%). The mineral is not homogeneous in respect of the distribution of some of its important elements like ThO₂ (nil–3.30%), Pr₂O₃ (nil–3.87%) and Y₂O₃ (nil–6.67%). While, Sm₂O₃, Gd₂O₃, UO₂ and SiO₂ are absent. Xenotime contains mainly Y (51.82–53.26%), P (15.34–15.64%) and O (34.19–34.23%).

Monazite and xenotime, although occur as accessory minerals, their consistent association with auriferous zones of Gadag field and elsewhere suggests a possible genetic relationship between monazite, xenotime and gold mineralization, hence they yield precise age of gold mineralization event (Pan and Fleet, 1990; Ugarkar et al., 2007). The occurrence of monazite from the auriferous zones of Gadag was first reported by Ugarkar et al. (2007). Subsequently, U–Pb dating of monazite and xenotime from the auriferous zones of Gadag by Sarma et al. (2011) has yielded 2522 ± 6 Ma for event of gold mineralization.

8.2. Ore minerals

Gold in the native form occurs as dispersed minute blebs, irregular patches and tiny stringers within quartz veins as well as altered wall-rocks. It occurs as tiny blebs within quartz (Fig. 6a), silicate minerals and sulfides, especially arsenopyrite (Fig. 6b). It is also evident from the ore microscopy and electron microprobe analysis that gold occurs

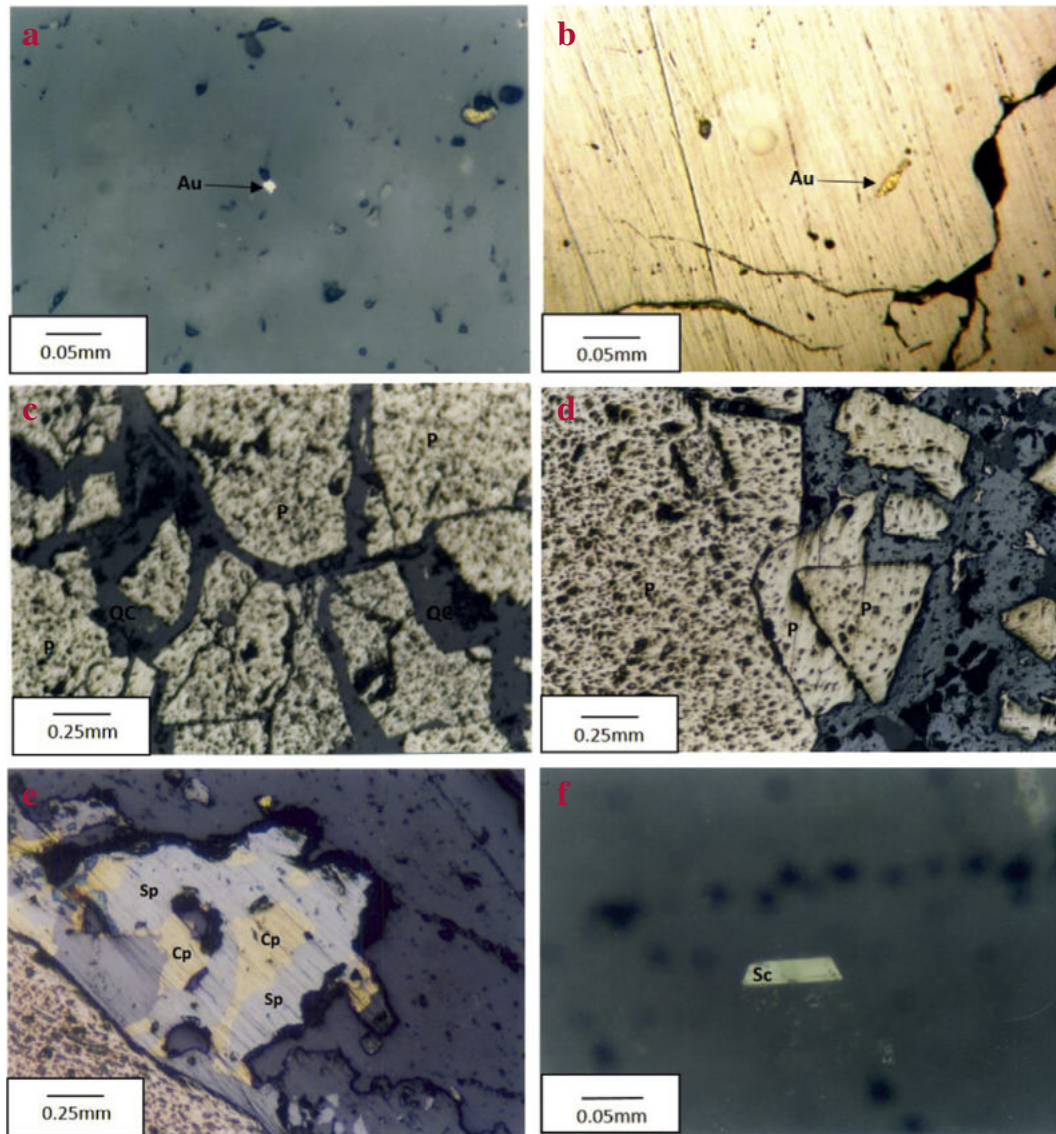


Fig. 6. Photomicrographs of ore minerals of the auriferous zones: (a) A bleb of native gold (Au) in the vein quartz. (b) Native gold inclusion (Au) within the arsenopyrite. (c) Fractures within pyrite (P) healed by quartz and carbonates (QC). (d) Individual pyrite crystals (P) interpenetrating due to deformation. (e) Chalcopyrite (Cp) and sphalerite (Sp) intergrown with each other. (f) Occurrence of scheelite (Sc) crystal within vein quartz.

in the turbidite hosted auriferous zones of Gadag not only in visible native state, but also in invisible state within arsenopyrite crystals (Ugarkar et al., 1994).

Arsenopyrite constitutes about 30% of the total sulfide mineral assemblage in the auriferous zones. Dimension varies from microscopic to as large as 10 mm in length, while the shape varies from anhedral to perfectly euhedral forms (Fig. 4e). Euhedral grains display shapes of rhombohedral, tabular, columnar, needle-like slender prismatic forms. At places, arsenopyrite crystals are deformed and fractured that are often healed by fibrous and banded quartz and carbonates. Arsenopyrites of bigger dimensions have inclusions of chalcopyrite of various sizes and shapes and occasionally tiny gold particles (Fig. 6b). Apart from chalcopyrite, arsenopyrite also has inclusions of sphalerite, galena, pyrrhotite, carbonate and quartz and chlorite. Arsenopyrite grains of study area compositionally contain Fe (34.70%), As (42.91–43.22%) and S (21.11–21.40%).

Electron microprobe data on arsenopyrite (Table 1) reveals that the gold values (0.23 to 0.34%) do not correspond to gold inclusions. Even at very high magnification, up to 20,000 times, gold particles are not seen at analytical spots in the arsenopyrite, hence it has been suggested by

Ugarkar et al. (1994) that at least a part of such gold recorded in the arsenopyrite is in solid solution and structure bound (Cabri et al., 1989) and rest could exist as ultrafine particles.

Pyrite is another most abundant sulfide mineral in the ore quartz veins and their associated wall rock alterations. Pyrite is mostly anhedral to subhedral, although at places it is euhedral in form. They are spongy in appearance and are commonly fractured, such fractures are healed by quartz and carbonate (Fig. 6c). At places, individual pyrite crystals are seen interpenetrating due to deformation effect (Fig. 6d). Electron microprobe analysis of a pyrite grain from central auriferous zone shows 46.66% of Fe and 22.64% of S.

Pyrrhotite occurs as isolated or individual grains, both in ore vein quartz and alteration zones. Its occurrence is lesser when compared with pyrite and arsenopyrite. At places, it occurs as inclusions in pyrite, arsenopyrite and quartz.

Chalcopyrite, although is in less abundance, it occurs invariably in the auriferous zone. At places, it occurs as remobilized tiny veins or fracture filling in silicate and sulfide minerals. It exhibits intergrowth texture with sphalerite (Fig. 6e). Electron microprobe analysis of a chalcopyrite grain shows the composition of 33.59% Cu, 30.55% Fe and 33.69% S.

Table 2
Chemical compositions of altered host rocks of the turbidite-hosted auriferous zone of Gadag gold field.

Sample	Silicified-carbonatized + sericitized host rock (SCS)							Chloritized-sericitized ± carbonatized host rock (CSC)					LATG*
	A1	A2	A3	A4	A5	A6	Av.	B1	B2	B3	B4	Av.	Av.
SiO ₂	70.8	69.03	69.44	69.63	66.89	69.29	69.18	53.31	55.21	53.98	54.86	54.34	60.67
TiO ₂	0.8	0.63	0.72	0.82	0.93	0.87	0.8	0.94	1.25	1.02	0.87	1.02	0.76
Al ₂ O ₃	11.57	11.11	11.78	12.28	13.05	12.87	12.11	21.47	24.89	12.94	13.54	18.21	15.31
Fe ₂ O ₃	3.62	2.48	3.84	2.9	2.29	2.73	2.98	13.67	6.83	15.52	16.18	13.05	12.02
MnO	0.15	0.19	0.28	0.14	0.28	0.22	0.21	0.03	0.01	0.18	0.17	0.1	0.18
MgO	3.36	3.82	3.56	4.3	3.58	3.46	3.68	2.48	1.12	4.28	2.89	2.69	2.87
CaO	3.12	6.47	4.5	3.52	5.6	5.23	4.74	0.4	0.17	4.18	2.68	1.86	3.16
Na ₂ O	1.09	0.92	0.88	0.67	0.95	0.74	0.88	1.33	1.02	0.71	0.96	1.01	1.15
K ₂ O	3.29	3.59	3.86	4.42	5.12	6.08	4.39	4.16	5.18	3.38	4.26	4.25	2.3
P ₂ O ₅	0.04	0.14	0.09	0.05	0.06	0.1	0.08	0.06	0.04	0.1	0.12	0.08	0.07
Ba	88	86	88	86	97	86	88	162	355	97	86	175	220
Rb	9	11	9	11	23	11	12	28	156	23	11	54	92
Sr	27	14	27	14	41	14	23	20	46	41	14	30	64
Cs	0.36	0.61	0.36	0.61	0.78	0.61	0.56	2.05	5.97	0.78	0.61	2.35	5.59
Ga	3.25	2.68	3.25	2.68	5.48	2.68	3.34	14.04	24.06	5.48	2.68	11.57	23
Ta	0.42	0.05	0.42	0.05	0.11	0.05	0.18	0.55	0.79	0.11	0.05	0.38	0.64
Nb	0.96	0.85	0.96	0.85	1.73	0.85	1.03	5.91	6.93	1.73	0.85	3.86	10
Hf	0.55	0.51	0.55	0.51	1.1	0.51	0.62	4.78	5.23	1.1	0.51	2.91	15
Zr	21	19	21	19	37	19	23	150	179	37	19	97	110
Y	11	12	15	11	13	17	13	15	15	9	12	13	33
Th	7.2	4.24	7.66	5.63	3.94	4.4	5.51	7.8	5.55	8.86	4.63	6.71	4.55
U	2.1	0.75	2.1	0.75	0.54	0.75	1.17	1.92	1.48	0.54	0.75	1.17	1.25
Cr	165	310	208	210	220	296	235	293	163	198	181	209	80
Ni	146	149	132	118	149	113	135	40	26	141	136	86	35
Co	33	29	37	45	35	40	37	10	6	45	42	26	48
Sc	4	4	4	9	4	9	6	15	24	9	4	13	8
V	191	165	194	217	188	190	191	104	196	114	207	155	178
Cu	119	124	84	95	180	142	124	40	19	113	187	90	95
Pb	8	10	24	19	8	19	14	5	4	24	19	13	6
Zn	70	98	115	97	120	86	98	47	42	75	88	63	53
Au	0.98	9.21	1.87	2.03	4.72	3.49	3.72	0.12	0.22	0.18	0.19	0.18	
As	330	7598	839	799	5418	4662	3274	148	166	187	203	176	
Sb	12	17	19	14	14	17	16	10	15	9	16	12.5	
La	7.86	5.93	6.88	7.64	2.95	3.48	5.79	27.36	24.06	27.56	24.54	25.88	24.44
Ce	11.77	7.88	8.32	14.89	5.95	6.59	9.23	49.47	43.94	49.44	43.24	46.52	44.97
Pr	0.84	0.81	0.74	1.61	0.65	0.76	0.9	6.11	5.56	6.14	5.63	5.86	5.06
Nd	5.23	4.11	3.85	6.69	2.67	3.15	4.28	22.65	21.14	22.17	21.68	21.91	18.51
Sm	0.91	0.84	0.74	1.3	0.5	0.77	0.84	4.65	4.39	4.5	4.22	4.44	3.77
Eu	0.19	0.16	0.12	0.2	0.09	0.13	0.15	0.94	1.12	0.88	1.01	0.99	1.05
Gd	0.67	0.78	0.65	0.93	0.42	0.62	0.68	3.36	3.09	3.31	2.99	3.19	3.26
Tb	0.11	0.09	0.1	0.13	0.07	0.12	0.1	0.56	0.51	0.5	0.51	0.52	0.62
Dy	0.63	0.56	0.68	0.79	0.44	0.72	0.64	2.88	2.71	2.58	2.56	2.68	3.91
Ho	0.07	0.08	0.08	0.09	0.06	0.09	0.08	0.56	0.59	0.54	0.6	0.57	0.8
Er	0.26	0.23	0.3	0.29	0.18	0.32	0.26	1.71	1.78	1.7	1.8	1.75	2.32
Tm	0.03	0.03	0.04	0.04	0.02	0.04	0.03	0.32	0.35	0.32	0.34	0.33	0.41
Yb	0.33	0.43	0.51	0.4	0.26	0.53	0.41	2.06	2.32	2.04	2.21	2.16	2.51
Lu	0.07	0.05	0.07	0.06	0.05	0.08	0.06	0.34	0.39	0.33	0.4	0.37	0.41
ΣREE	28.97	21.98	23.08	35.06	14.31	17.4	23.47	123	112	122	111.7	117.2	112.04
LREE	26.8	19.73	20.65	32.33	12.81	14.88	21.2	111.2	100.2	110.7	100.3	105.6	97.8
HREE	2.17	2.25	2.43	2.73	1.5	2.52	2.27	11.79	11.74	11.32	11.41	11.57	14.24
LREE/HREE	12.35	8.77	8.5	11.84	8.54	5.9	9.32	9.43	8.54	9.78	8.79	9.14	6.86
La _N /Yb _N	16.1	9.32	9.12	12.91	7.67	4.44	9.93	8.98	7.01	9.13	7.5	8.16	6.64
Ce _N /Yb _N	9.24	4.75	4.23	9.65	5.93	3.22	6.17	6.22	4.91	6.28	5.07	5.62	4.67
Gd _N /Yb _N	1.65	1.47	1.03	1.88	1.31	0.95	1.38	1.32	1.08	1.32	1.1	1.21	1.06

* LATG: Least altered turbidite greywacke of Gadag gold field.

Sphalerite is a minor sulfide mineral that occurs in the auriferous zone. It is subhedral to anhedral in form and gray in color with internal reflections. It is distributed as minute blebs and amoeba like forms in the silicate gangue and at places in arsenopyrite. It is normally associated with chalcopyrite. Mutual boundary textures as well as intergrowth textures are seen between sphalerite and chalcopyrite (Fig. 6e).

Galena, like sphalerite, is also a minor sulfide mineral in the auriferous zone. It occurs in anhedral form especially in ore vein quartz. At places, it is seen to occupy space between grains of silicate minerals. Individual blebs of galena are seen scattered in the silicate gangue.

Scheelite with grayish white subhedral to euhedral prismatic and tubular form occurs especially in quartz veins (Fig. 6f). Tiny long specks

of scheelite inclusions occur in arsenopyrite crystals. It has a distinct internal reflection and majority of crystals exhibit polysynthetic twinning.

9. Geochemistry of Central Auriferous Zone

Hydrothermal alterations causing silicification, carbonatization, chloritization, sericitization and sulfidation in the host graywacke have significantly modified the original composition of the precursor host rock. Compositional variations of major, trace and rare earth elements as well as gold in the altered wall rocks, namely silicified + carbonatized + sericitized rock and chloritized-sericitized ± carbonatized rock from Mysore underground mine faces and drill core representing the hydrothermally altered wall rocks at Central

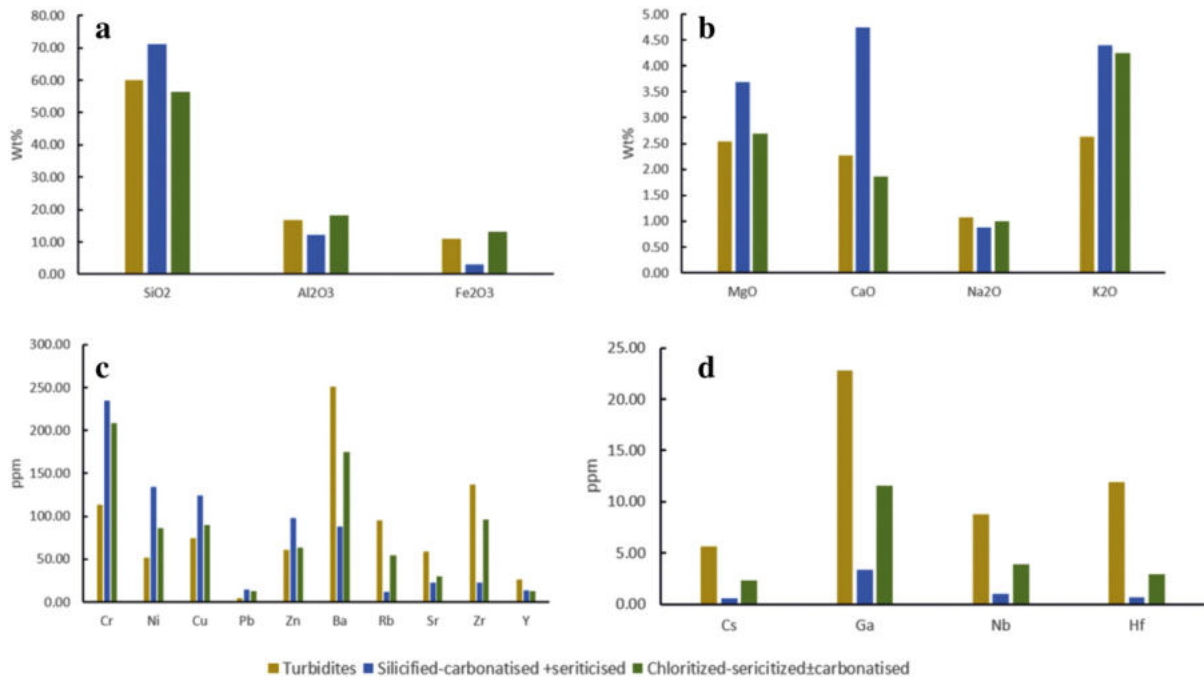


Fig. 7. Histograms showing relative abundances of major and trace elements in the altered wall rocks of auriferous zones and the least altered host rocks of Gadag greenstone belt.

Auriferous Zone, along with the composition of least altered host turbidite graywacke for comparison, are given in Table 2.

9.1. Major and trace element geochemistry

In the silicified + carbonatised + sericitized wall rock (SCS) immediately proximal to auriferous quartz veins, silicification/quartz veining and carbonitization have elevated SiO₂ (69.18 wt.%), MgO (3.68 wt.%), CaO (4.74 wt.%) and K₂O (4.39 wt.%) contents (Table 2) compared to their background values in the least altered turbidite graywacke (60.67 wt.%, 2.87 wt.%, 3.16 wt.% and 2.30 wt.% respectively) (Fig. 7a, b). The samples with elevated contents of SiO₂, CaO and MgO contain abundant quartz and ankerite, while the elevated values of K₂O are due to the presence of sericite. Alterations have apparently diluted the relative abundance of other major oxides like, Al₂O₃ (12.11 wt.%), Fe₂O₃ (2.98 wt.%) and Na₂O (0.88 wt.%) in the altered wall rocks compared to these oxides in the least altered host rock (15.31 wt.%, 12.02 wt.% and 1.15 wt.% respectively). Trace elements, like Cr (235 ppm), Ni (135 ppm), Cu (124), Pb (14 ppm) and Zn (98 ppm) are elevated in the altered wall rocks, compared to their values in the least altered host rock (80 ppm, 35 ppm, 95 ppm, 6 ppm and 53 ppm respectively, Fig. 7c, d), which could be due to the development of sulfides in this zone. The elements like, Ba (88 ppm), Rb (12 ppm), Sr (23 ppm), Cs (0.56 ppm), Ga (3.34 ppm), Nb (1.03 ppm), Hf (0.62 ppm), Zr (23 ppm) and Y (13 ppm) are depleted compared to their values in the least altered host rock (220 ppm, 92 ppm, 64 ppm, 5.59 ppm, 23 ppm, 10 ppm, 15 ppm, 110 and 33 ppm respectively, Fig. 7c, d). The abundance of these elements in the least altered rocks is probably held in clay matrix, lithic fragments and plagioclase feldspar, which are diluted due to hydrothermal alterations. Au contents in this zone vary between 0.98, 4.72 ppm, and 0.49 ppm and As contents are high (330–7598 ppm), due to the presence of arsenopyrites in this zone.

In the chloritized–sericitized ± carbonatised wall rock (CSC) next to SCS wall rock, Al₂O₃ (18.21 wt.%) and K₂O (4.25 wt.%) are elevated, while SiO₂ (54.34 wt.%) and CaO (1.86 wt.%) contents are depleted (Table 2), compared to their values in the least altered host rock (15.31 wt.%, 2.30 wt.%, 60.67 wt.% and 3.16 wt.% respectively, Fig. 7a, b). This variation could be due to the abundance of chlorite and sericite in this zone. Fe₂O₃ (13.05 wt.%), MgO (2.69 wt.%) and Na₂O (1.01 wt.%)

contents are consistent with their values in the least altered host graywacke. Trace elements like Cr (209 ppm), Ni (86 ppm), Pb (13 ppm), Nb (3.86 ppm), Th (6.71 ppm), and Sc (13 ppm) are elevated in the altered wall rocks, compared to their values in the least altered host rock (80 ppm, 35 ppm, 95 ppm, 6 ppm and 10 ppm, 4.55 ppm and 8 ppm respectively, Fig. 7c, d), which could be due to the development of chlorite, sericite and sulfides in the altered zone. The elements like Ba (175 ppm), Rb (54 ppm), Sr (30 ppm), Cs (2.35 ppm), Ga (11.57 ppm), Nb (3.86 ppm), Hf (2.91 ppm), Zr (97 ppm) and Y (13 ppm) and Co (26 ppm) are depleted compared to their values in the least altered host rock (220 ppm, 92 ppm, 64 ppm, 5.59 ppm, 23 ppm, 10 ppm, 15 ppm, 110, 33 ppm 48 ppm respectively, Fig. 7c, d). The abundances of these elements in the least altered rocks are probably held in clay

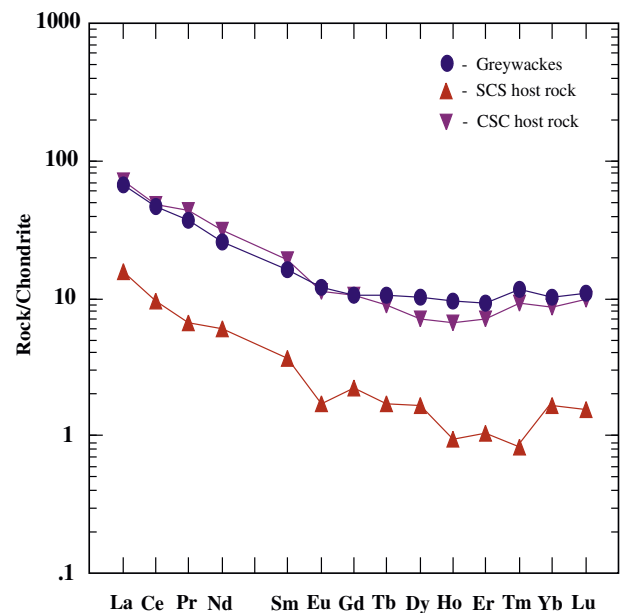


Fig. 8. Chondrite normalized patterns of average REE values of altered wall rocks of auriferous zones and the least altered turbidite graywackes of Gadag gold field.

matrix, lithic fragments and plagioclase feldspar, which are diluted due to hydrothermal alterations. Au content in this zone varies from 0.12 to 0.22 ppm, while As content varies from 148 to 208 ppm.

9.2. Rare earth element geochemistry

Rare earth element geochemistry has been widely applied in recent years to model ore genesis for a variety of mineral deposits as large amount of data is available on the REE abundances of the

whole rock and ores (Kerrick and Fryer, 1979; Campbell et al., 1984; Pan et al., 1994; Giritharan and Rajamani, 2001; Sarangi et al., 2013). However, not much information is available on the REE geochemistry of Archean turbidite hosted auriferous zones.

The behavior of REE during hydrothermal alterations in the gold deposits of Archean greenstone belts of India studied by Giritharan and Rajamani (2001), Manikyamba et al. (2004) and Ugarkar and Natikar (2011) is limited to only few deposits, and is confined to metavolcanic hosted deposits of Kolar, Hutti, Penakacherla and Gadag gold fields of

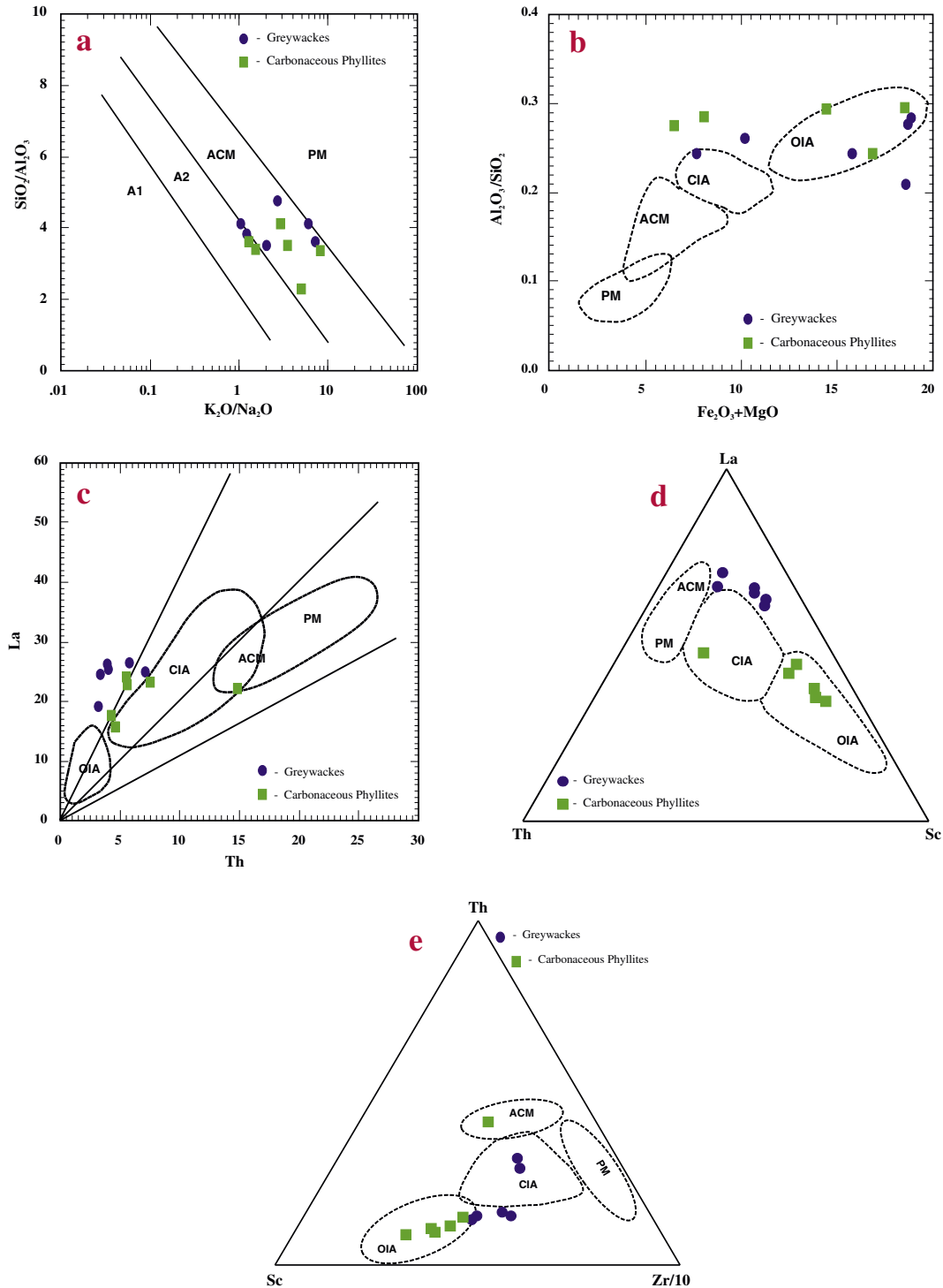


Fig. 9. (A) $\text{SiO}_2/\text{Al}_2\text{O}_3$ – $\text{K}_2\text{O}/\text{Na}_2\text{O}$, (B) $\text{Al}_2\text{O}_3/\text{SiO}_2$ – $\text{Fe}_2\text{O}_3 + \text{MgO}$, (C) La–Th, (D) La–Th–Sc and (E) Th–Sc–Zr/10 tectonic discrimination diagrams (after Bhatia and Crook, 1986) for the least altered turbidite sequence of Gadag gold field.

Table 3
Chemical compositions of least altered graywackes and carbonaceous phyllites of Gadag gold field.

Sample	Graywackes							Carbonaceous phyllites						
	G1	G2	G3	G4	G5	G6	Av.	CP1	CP2	CP3	CP4	CP5	CP6	Av.
SiO ₂	65.82	63.29	57.85	58.70	60.56	57.80	60.67	55.06	61.49	62.43	55.11	57.21	65.72	59.50
TiO ₂	0.35	0.47	0.99	0.74	0.87	1.16	0.76	1.10	1.10	0.12	0.64	1.25	1.21	0.90
Al ₂ O ₃	16.02	16.51	16.03	14.28	12.66	16.37	15.31	16.26	14.97	17.20	16.17	24.89	18.78	18.05
Fe ₂ O ₃	5.44	7.69	15.39	12.20	15.98	15.42	12.02	15.55	13.79	5.90	9.82	6.83	6.86	9.79
MnO	0.09	0.12	0.20	0.20	0.31	0.18	0.18	0.27	0.05	0.02	0.20	0.01	0.01	0.09
MgO	2.17	2.44	3.20	3.50	2.54	3.37	2.87	2.90	2.96	0.52	4.53	1.12	1.14	2.20
CaO	3.72	3.40	0.93	6.21	4.20	0.51	3.16	0.61	0.34	0.69	6.24	0.17	0.14	1.37
Na ₂ O	2.48	2.12	0.42	0.34	0.41	1.13	1.15	0.43	0.54	1.63	1.40	1.02	0.89	0.99
K ₂ O	2.63	2.61	3.02	2.07	1.13	2.35	2.30	3.59	1.58	2.09	2.19	5.18	3.12	2.96
P ₂ O ₅	0.07	0.07	0.04	0.06	0.12	0.07	0.07	0.07	0.08	0.01	0.04	0.04	0.03	0.05
LOI	1.12	1.15	1.82	1.64	1.07	1.53	1.39	3.90	2.67	4.68	3.02	1.48	1.59	2.89
Total	99.91	99.87	99.89	99.93	99.85	99.89	99.89	99.74	99.57	99.07	99.36	99.20	99.49	99.41
Ba	248	283	174	157	168	292	220	405	170	241	292	355	228	282
Rb	101	104	116	68	46	115	92	166	66	66	51	156	91	99
Sr	83	86	34	61	66	51	64	50	33	65	91	46	43	55
Cs	4.60	4.67	10.19	5.74	2.87	5.44	5.59	6.86	4.45	6.11	5.09	5.97	5.25	5.62
Ga	21	21	23	19	25	30	23	26	29	18	16	24	20	22
Ta	0.89	0.57	0.59	0.41	0.59	0.78	0.64	0.78	0.57	0.95	0.19	0.79	0.96	0.71
Nb	11	8	10	8	11	14	10	9	9	6	5	7	7	7
Hf	16	14	18	12	13	15	15	6	6	5	4	5	27	9
Zr	101	96	140	98	104	119	110	199	211	115	145	179	131	163
Y	31	32	35	35	34	32	33	18	27	15	18	15	21	19
Th	7.09	5.80	3.90	3.15	3.31	4.02	4.55	5.62	7.51	14.86	4.63	5.55	4.26	7.07
U	2.04	1.67	0.85	1.01	0.95	0.99	1.25	1.41	2.38	4.31	1.42	1.48	1.51	2.09
Cr	42	47	114	80	76	119	80	106	210	64	148	163	191	147
Ni	16	23	50	31	40	51	35	116	99	33	73	26	62	68
Co	12	16	80	41	65	73	48	60	43	9	34	6	25	29
Sc	6	5	9	7	11	12	8	32	25	10	25	24	30	24
V	64	82	221	165	270	268	178	252	205	45	167	196	233	183
Cu	59	83	137	71	116	102	95	116	84	19	34	19	52	54
Pb	7.10	7.35	4.62	5.48	4.20	4.29	5.51	4.13	6.06	3.99	4.15	3.86	3.58	4.30
Zn	37	38	51	41	75	79	53	97	165	26	43	42	40	69
Sample	Turbidite-Greywacke							Carbonaceous Phyllite						
	G1	G2	G3	G4	G5	G6	Av.	CP1	CP2	CP3	CP4	CP5	CP6	Av.
Zr/Y	3.26	3.00	4.00	2.80	3.06	3.72	3.33	10.84	7.71	7.41	8.06	12.03	6.32	8.54
Zr/Th	14.25	16.55	35.90	31.11	31.42	29.60	24.18	35.46	28.09	7.72	31.39	32.33	30.69	23.11
Th/U	3.48	3.47	4.59	3.12	3.48	4.06	3.64	3.99	3.16	3.45	3.26	3.75	2.82	3.39
Th/Sc	1.18	1.16	0.43	0.45	0.30	0.34	0.57	0.17	0.30	1.55	0.19	0.23	0.14	0.29
Zr/Sc	16.83	19.20	15.56	14.00	9.45	9.92	13.75	6.19	8.47	11.94	5.92	7.35	4.38	6.74
La	25.06	26.4	26.23	19.12	24.49	25.33	24.44	22.82	23.35	22.16	15.71	24.06	17.61	20.95
Ce	44.27	45.83	50.19	34.59	47.77	47.17	44.97	43.33	45.64	37.57	31.53	43.94	30.76	38.80
Pr	4.76	4.87	5.77	3.89	5.6	5.47	5.06	5.49	5.68	4.22	4.08	5.56	3.65	4.78
Nd	16.18	16.85	21.55	14.69	21.58	20.21	18.51	21.29	21.71	14.3	16.5	21.14	13.79	18.12
Sm	3.21	3.15	4.21	3.11	4.59	4.36	3.77	4.66	4.68	2.76	3.69	4.39	2.57	3.79
Eu	0.93	0.89	1.07	0.95	1.24	1.2	1.05	1.31	0.94	0.57	1.03	1.12	0.77	0.96
Gd	3.23	3.1	3.47	2.72	3.55	3.47	3.26	3.81	3.85	2.42	3.14	3.09	2.48	3.13
Tb	0.62	0.59	0.64	0.58	0.64	0.64	0.62	0.62	0.75	0.42	0.6	0.51	0.53	0.57
Dy	4.12	3.75	4.08	3.98	3.68	3.87	3.91	3.52	4.81	2.66	3.52	2.71	3.57	3.47
Ho	0.81	0.74	0.87	0.83	0.8	0.77	0.8	0.75	1.04	0.59	0.72	0.59	0.83	0.75
Er	2.22	2.09	2.62	2.31	2.38	2.31	2.32	2.21	3.04	1.66	1.9	1.78	2.41	2.17
Tm	0.39	0.35	0.44	0.41	0.44	0.44	0.41	0.41	0.58	0.31	0.36	0.35	0.47	0.41
Yb	2.13	2.31	2.83	2.54	2.68	2.58	2.51	2.7	3.53	2	2.11	2.32	2.83	2.58
Lu	0.36	0.33	0.46	0.4	0.44	0.44	0.41	0.43	0.55	0.31	0.34	0.39	0.46	0.41
ΣREE	108.29	111.25	124.43	90.12	119.88	118.26	112.04	113.35	120.15	91.95	85.23	111.95	82.73	100.89
LREE	94.41	97.99	109.02	76.35	105.27	103.74	97.8	98.9	102	81.58	72.54	100.21	69.15	87.40
HREE	13.88	13.26	15.41	13.77	14.61	14.52	14.24	14.45	18.15	10.37	12.69	11.74	13.58	13.50
LREE/HREE	6.8	7.39	7.07	5.54	7.21	7.14	6.86	6.84	5.62	7.87	5.72	8.54	5.09	6.61
La/Sc	4.18	5.28	2.91	2.73	2.23	2.11	3.06	0.71	0.94	2.31	0.64	0.99	0.59	0.86
La/Th	3.53	4.55	6.73	6.07	7.40	6.30	5.37	4.06	3.11	1.49	3.39	4.34	4.13	2.96
La/Y	0.81	0.83	0.75	0.55	0.72	0.79	0.74	1.24	0.85	1.43	0.87	1.61	0.85	1.09
La _N /Yb _N	7.95	7.72	6.26	5.09	6.18	6.63	6.64	5.71	4.47	7.49	5.03	7.01	4.2	5.65
Ce _N /Yb _N	5.39	5.14	4.6	3.53	4.62	4.74	4.67	4.16	3.35	4.87	3.87	4.91	2.82	4.00
Gd _N /Yb _N	1.23	1.09	0.99	0.87	1.07	1.09	1.06	1.14	0.88	0.98	1.21	1.08	0.71	1.00

Dharwar Craton. Their study has indicated evidences of varying extents of LREE addition to the altered host rocks immediately proximal to the auriferous quartz veins.

The chondrite normalized REE patterns of average values of least altered turbidite graywacke and altered wall rocks are plotted to get a distinct pattern (Fig. 8). The REE geochemistry of host turbidite

graywacke (least altered) and alteration zones of Central Auriferous Zone has shown distinct characteristics. The average contents of Σ REE, Σ LREE and Σ HREE of SCS wall rock (23.47 ppm, 21.20 ppm and 2.27 ppm respectively) are significantly less when compared to the least altered graywacke (112.04 ppm, 97.80 ppm and 14.24 ppm respectively), while CSC wall rock does not exhibit notable variation in

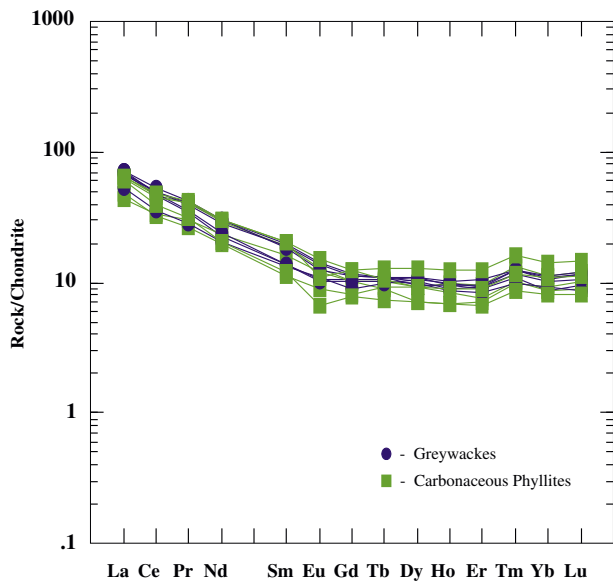


Fig. 10. Chondrite normalized REE patterns of the least altered turbidite graywackes of Gadag gold field.

these contents (117.17 ppm, 105.60 ppm and 11.57 ppm respectively). The observed lower abundances of REE in the SCS wall rock are due to extensive silicification and carbonatization of host rock. The average value of LREE/HREE ratio in the least altered host is 6.86, while in SCS is 9.32 and in CSC rock is 9.14. The chondrite normalized REE pattern of the least altered host graywacke exhibits enrichment of LREE over HREE ($La_N/Yb_N = av. 6.64$) without any Eu anomaly, so also in CSC ($La_N/Yb_N = av. 8.16$), while in SCS also it exhibits enriched LREE ($La_N/Yb_N = av. 9.93$), but with prominent negative Eu anomaly (Fig. 8).

10. Geodynamic setting

Orogenic gold deposits dominantly form in metamorphic rocks in the mid-to shallow crust (5–15 km depth), at or above the brittle ductile transition, in compressional subduction-accretion geodynamic settings that facilitate transfer of hot gold bearing fluids from deeper levels (Goldfarb et al, 2005; Kerrich et al., 2000; Phillips and Powell, 2009).

Major elements like SiO_2 , Al_2O_3 , Fe_2O_3 , MgO , K_2O , and Na_2O , certain trace elements such as Zr, La, Th, Sc, Nb, REE and Zr/Y, Zr/Th, Th/Sc, La/Sc, La/Th and Th/U of clastic sediments are variable along with different types of geodynamic settings, hence they have been widely used to determine tectonic settings of clastic sedimentary rocks (Bhatia, 1983, 1985; Taylor and McLennan, 1985; Bhatia and Crook, 1986; Roser and Korsch, 1986; McLennan et al., 1990). The least altered graywackes and carbonaceous phyllites of Gadag greenstone belt have moderate SiO_2/Al_2O_3 and K_2O/Na_2O values, moderate to high Al_2O_3/SiO_2 and $Fe_2O_3 + MgO$ values, thus indicating that these sediments deposited in a subduction related tectonic settings like oceanic island arc, continental island arc and active continental margin (Fig. 9a and b). Bhatia and Crook (1986) have inferred the tectonic settings of clastic sediments by using various element compositions and their ratios. The Zr (110 ppm), La (24.44 ppm), Th (5 ppm), Sc (8 ppm) and Nb (10 ppm) contents and Zr/Y (3.33), Zr/Th (22), Th/Sc (0.63), La/Sc (3.15), La/Th (4.89) and Th/U (3.64) ratios of graywackes and Zr (163 ppm), La (20.95 ppm), Th (7 ppm), Sc (24 ppm) and Nb (9 ppm) contents and Zr/Y (8.57), Zr/Th (23.38), Th/Sc (0.29), La/Sc (0.87), La/Th (3.80) and Th/U (3.34) ratios of carbonaceous phyllite of Gadag belt (Table 3) closely match the values of clastic sediments deposited mainly in subduction related continental island arc and active continental margin geodynamic settings. In La–Th, La–Th–Sc and Th–Sc–Zr/10

ternary diagrams (Fig. 9c, d and e) of Bhatia and Crook (1986), the plots of least altered turbidite sequence of Gadag belt indicate continental island arc and oceanic arc tectonic settings for their deposition.

The average REE pattern of graywackes and carbonaceous phyllites of Gadag gold field is similar to that of Type 1 plot of Archean turbidites (McLennan and Taylor, 1991) with LREE enrichment, flat HREE ($Gd_N/Yb_N = 1.0–2.0$) and without or slight, negative Eu anomalies (Fig. 10). Such patterns may be derived by mixing of a bimodal igneous suite and/or by sources with intermediate REE patterns, such as those commonly found at modern island arcs (McLennan and Taylor, 1991). On the other hand, the REE pattern of Gadag turbidite sequence resembles those typical of modern deep-sea turbidites from various active margin tectonic settings (McLennan et al., 1990) suggesting their derivation from the upper continental crust and their deposition in active continental margins related to subduction of plates (Taylor and McLennan, 1985). Compressional subduction tectonic setting is also evident from the thickening of Gadag greenstone belt due to overturning on large scale folds and stacking on reverse faults in a duplex, comprising tectonic domains (horses or thrust slices) separated by discontinuities/thrusts (Chadwick et al., 2003). Based on the geologic setting, major and selected trace element modeling of various clastic metasediments of Gadag belt, Ugarkar and Nyamati (2002) suggested that the various clastic metasedimentary rocks exhibiting compositional diversity and different tectonic settings might have been juxtaposed as accretionary prisms by convergent margin processes.

11. Discussion

The vast majority of orogenic gold deposits occur in three periods in geologic time; the Neoproterozoic (ca. 2700–2400 Ma), a second period is in the Paleoproterozoic (ca. 2100–1800 Ma) and a third period from ca. 650 Ma continuing throughout the Phanerozoic (Goldfarb et al., 2001). The reason for this could be that these major periods of formation coincided with periods of subduction related accretionary tectonics and continental growth (Goldfarb et al., 2001). The characteristics of Neoproterozoic gold deposits are common to the lode gold deposits of subduction complexes of Pacific Margin (Barley et al., 1989; Goldfarb et al., 1998). Orogenic gold deposits are associated with, or located adjacent to the first order, deep trans-crustal fault zones generally terrain-bounding, or docking structure that remark the boundaries of distinct, tectonically juxtaposed metamorphosed supracrustal terrains (Wyman and Kerrich, 1988; Kerrich et al., 2000; Goldfarb et al., 2005; Tomkins, 2014). Fluid migration along such zones was driven by episodes of major pressure fluctuations during seismic events. Ores formed as vein fill of second and third order shears and faults, particularly at jogs or changes in strike along the crustal fault zones as strike-slip thrust. Although spatially and temporally associated with structures of regional extent, orogenic gold deposits are rarely located within the first order structures, but instead are hosted in second or third order splays of the regional structures (Kerrich et al., 2000; Goldfarb et al., 2005).

In models to evolve orogenic deposits, the generation of fluid phase takes place by pore fluid devolatilization and dehydration-decarbonatization reactions associated with prograde metamorphism of oceanic slab. Prograde dehydration and decarbonatization reactions of carbonate enriched oceanic crust of the slab typically produce CO_2 -rich aqueous phases (Elder and Cashman, 1992). There is a possibility that some of the shear zones of gold mineralization may penetrate to the depth of the mantle (Kerrich et al., 2000). The world class gold deposits of Abitibi belt are probably formed through a process of mantle plume-island arc accretion (Barley et al., 1998; Wyman et al., 1999), suggesting that the source of the gold bearing fluids may anywhere from mantle to crust (Santosh, 1993). Based on the $\Delta^{33}S$ signature of sulfur in four Archean orogenic gold deposits, Xue et al. (2013) have suggested a granitic source for hydrothermal fluids. The gold deposits

that have many aspects in common, irrespective of time and space, led Groves et al. (1998) to classify them collectively as orogenic gold deposits. Temporal relationship between gold mineralization, alteration, metamorphism and deformation is generally compatible for volcanics, turbidite–slate and other host rocks for lode deposits of Archean greenstone belts (Groves et al., 1998; McCuaig and Kerrich, 1998). Although, gold deposits hosted by turbidites have wide distribution throughout the world, occurring in rocks ranging in age from Archean to Tertiary, their abundance is less compared to greenstone hosted gold deposits. However, turbidite hosted terrains have been important sources of gold, particularly in Victoria of Australia, Nova Scotia, Canada, SE Guizhou, China (Kontak et al., 1990; Cox et al., 1995; Lu et al., 2005). Deposits of this type occur in thick accretionary turbidite sequence (graywacke–mudstone), intruded by granitic plutons, and are in proximity to major crustal boundaries (Robert et al., 2007). The presence of a hydrated oceanic substrate is considered to be favorable for the development of well mineralized terrains (Bierlein et al., 2004). One of the most significant and consistent features of such deposits is that, the carbonaceous matter is so commonly associated with gold mineralization, is of sedimentary origin and forms an integral part of the host turbidite sequence (Bierlein et al., 1998, 2001; Ugarkar and Deshpande, 1999).

The regional structure of Gadag greenstone belt, as described by Narayanaswamy and Ahmed (1963) is an asymmetrical isocline with axial plane dipping to the east. In the widest part of Gadag belt, the lithological assemblage of volcano–sedimentary rocks is ~17 km thick (perpendicular to dip), and thickness is the result of overturning on large scale folds and stacking on reverse faults (Chadwick et al., 2003). Structural relationship between folding and faulting events in the Gadag belt indicates that the formation of fault zones (shear zones) broadly postdates fold development. However, shear zone probably formed late during the same regional deformation event which caused folding and associated cleavage development. The Gadag duplex, deformation, folds and reverse strike slip faults (discontinuities) were caused by the compression associated with subduction processes. The gold deposits are located near a 400 km long prominent crustal scale fault zone on eastern side of the Gadag duplex (Kaila et al., 1979; Chadwick et al., 2003). Such crustal scale faults have been proposed to penetrate very deep to tap CO₂ rich fluids from mantle (Pili et al., 1997; Goldfarb et al., 2005). The Gadag duplex as termed by Chadwick et al. (2003), comprises domains that are separated by over stacking discontinuities (thrusts). Such discontinuities interlinked with large scale thrusts might have acted as fluid paths leading to the precipitation of gold in sub-parallel to en-echelon splays of secondary or tertiary order as observed in gold deposits elsewhere (Kerrich et al., 2000; Goldfarb et al., 2005). Fluid activity may have been enhanced as a result of emplacement of granites adjacent to the Gadag greenstone belt.

The Central Auriferous Zone hosted in the turbidite sequence of Gadag belt is characterized by hydrothermal wall-rock alterations represented by chloritization, sericitization, carbonatization, silicification and sulfidation with ubiquitous association of carbonaceous matter. Notable distinctions in mineral assemblage, texture and in chemical compositions of altered wall rocks compared to the precursor host rock in the study area imply that metasomatism and wall rock alterations are the results of pervasive infiltration and intense interaction between hydrothermal fluids and the surrounding host rocks over prolonged period. Geochemical characters and mineralogical observations suggest the addition of sulfides, carbonates, carbonaceous matter, K₂O, MgO, CaO, Cr, Ni, Cu, Pb, Zn and As into altered wall rocks (SCS) immediately enveloping the auriferous quartz vein bodies. In this zone, gold values are also high (0.98–4.72 ppm). The \sum REE, \sum LREE and \sum HREE contents of SCS wall rock are significantly less when compared to the least altered host turbidite. The chondrite normalized REE pattern of SCS exhibits enriched LREE ($La_N/Yb_N = av. 9.93$), with prominent negative Eu anomaly. The observed variation in geochemical characteristics and mineral assemblages in alteration zone indicates differential response of the host rock and intensity of alteration depending on the

composition of host rocks and hydrothermal fluids. Further, these features of the altered wall rocks immediately adjacent to gold quartz veins strongly suggest that the hydrothermal fluids became more reduced during interaction with the wall rocks and carbonate precipitation.

Although orogenic gold deposits are hosted by metamorphic rocks of variable metamorphic grades, the event of ore formation most commonly postdates metamorphism of host rocks in the immediate vicinity (Goldfarb et al., 2005). The regional metamorphism and hydrothermal wall rock alterations are complex and complimentary processes and their relationship is an important aspect in the study of orogenic lode gold deposits. Generally, the former results in prograde metamorphism while latter leads to retrogression (Mueller and Groves, 1991; Ugarkar, 1998). In most of the orogenic deposits, gold mineralization occurs in greenschist to amphibolite facies of metamorphic domain, but the mineral assemblages in the mineralized zones are generally denoted by low-grade assemblage (Groves et al., 1987; Ugarkar, 1998; Goldfarb et al., 2005). A prominent feature of alteration associated with the gold mineralization is the widespread enrichment of carbonate in the alteration zones. This is consistent with alteration by infiltration of CO₂-bearing fluids. However, although rare, there are examples of gold mineralization in higher-grade assemblages like mid-upper amphibolite grade at Kolar deposit, India, upper amphibolite grade at Big Bell deposit, Yilgarn, Australia and granulite grade at Renco deposit, Zimbabwe (Hamilton and Hodgson, 1986; Kolb et al., 2000; Goldfarb et al., 2005).

The fluid inclusion studies carried out by us (Malapur et al., 2012) indicate three types of fluid inclusions, namely CO₂-rich inclusions, H₂O inclusions and CO₂-H₂O inclusions in the auriferous quartz veins of Central Auriferous Zone of the Gadag belt. The micro-thermometric measurements of these fluid inclusions indicate that the auriferous hydrothermal fluids were of low salinity (2.0 to 6.6 wt.% NaCl), dominated by CO₂-H₂O (about 30 mol% CO₂) with moderate densities (0.7 to 1.04 g/cm³), and gold deposition occurred over a wide temperature range of 175 to 325 °C. Metamorphism of host rocks at greenschist–amphibolite facies boundary with chlorite–calcite–quartz assemblage produces large volumes of low-salinity CO₂-H₂O fluids, similar in composition to those recorded in the Archean greenstone hosted vein type lode gold deposits (Groves and Foster, 1993; Kerrich and Cassidy, 1994). Further, it has been suggested that there is a close relationship between gold mineralization and retrograde greenschist facies metamorphism (Ugarkar, 1998). Retrograde metamorphism and corresponding mineral assemblages can be maintained during metamorphism in the presence of CO₂ dominance (Clark et al., 1986). Thus CO₂ seems to be an almost universal constituent of the ore fluids depositing gold and it forms a major constituent of most of fluid inclusions in gold ores from the metamorphic environment (Roedder, 1984). Progressive carbonization of wall-rocks with decreasing temperature and pressure might lead to fluid immiscibility and separate H₂O-rich and CO₂-rich phases (Groves and Foster, 1993). Reaction involving carbonate precipitation can substantially decrease XCO₂ in the fluids, and therefore fluids should evolve to more reduced, less CO₂-rich, CH₄-bearing compositions (Cox et al., 1995), as they react with carbonaceous wall rock (Bierlein et al., 2000). Gold occurs in quartz veins as well as altered wall rock envelope with carbonaceous matter, suggesting gold deposition being caused directly by redox reactions in the wall rock.

The zircon U–Pb dating ages of intrusive granites of Gadag greenstone belt have yielded 2555 ± 6 Ma, metavolcanics have yielded 2588 ± 10 Ma, while U–Pb dating of in-situ monazite of Central Auriferous Zone has yielded 2522 ± 6 Ma (Sarma et al., 2011). There was a gap of about 33 Ma between the intrusive magmatism and gold mineralization event. During the initial period of this gap regional metamorphism occurred in the entire greenstone belt, while during later period, hydrothermal fluids responsible for gold mineralization were probably derived from metamorphic processes as well as intrusive granites, and channeled through the thrust in the host turbidite rocks carrying

dissolved gold, associated metals and sulfur, which ultimately were precipitated in a reducing environment in the splays to the thrust in the Gadag duplex at about 2522 ± 6 Ma, resulting in retrograde alteration assemblages (Ugarkar, 1998; Sarma et al., 2011, 2012).

12. Conclusions

The gold mineralization in three auriferous zones hosted within the distinct lithological assemblages of metavolcanics and metasediments of the Archean Gadag greenstone belt resembles classic orogenic lode gold deposits. The Central Auriferous Zone, a main auriferous zone, is hosted mainly within the turbidites, comprising interbedded sequence of thick medium to coarse grained lithic graywacke and thin laminated layers of fine grained carbonaceous phyllite.

Parallelism between the linear strike-parallel distribution of auriferous zones, the axial trace of the syncline in the Central Auriferous Zone and the regional cleavages/schistosity points to a close relationship between the movement and focusing of gold bearing hydrothermal fluids, folding and cleavages/schistosity.

Notable distinctions in mineral assemblage, texture and in chemical compositions of altered wall rocks compared to the precursor host rock in the study area imply that metasomatism and wall rock alterations are the results of pervasive infiltration and intense interaction between hydrothermal fluids and the surrounding host rocks over a prolonged period.

The Gadag duplex, deformation, folds and reverse strike slip faults (discontinuities) were caused by the compression associated with subduction related tectonic processes. Mixing between $\text{CO}_2\text{-H}_2\text{O}$ fluids and more reduced fluids, which evolved during fluid reaction with adjacent carbonaceous wall rocks, channeled through the thrust in host turbidite sequence carrying dissolved gold, associated metals and sulfur, ultimately were precipitated in a reducing environment in the splays to the thrust in the Gadag duplex.

Acknowledgments

The authors are grateful to Drs. V. Balam, D.S. Sarma and M. Ram Mohan of National Geophysical Research Institute, Hyderabad for extending facilities to analyze the samples. We also express our indebtedness to Dr. T.C. Devaraju, late Dr. T.A. Alapieti and Dr. T.A.A. Halkoaho of University of Oulu, Linnanmaa, Finland for providing electron probe analytical data of our samples. A part of work was carried out under the CSIR Pool Scientistship awarded to the senior author (AGU). The authors also thank the Chairman, Department of Studies in Geology, Karnatak University, Dharwad for providing infrastructure facilities to carry out the present study. AGU thanks Dr. M. Santosh for inviting him to contribute a paper to this special issue of Ore Geology Reviews. The authors thank anonymous reviewer of this paper for valuable comments.

References

- Alapieti, T.T., Sivonen, S.J., 1983. Use of electron microprobe in the investigation of the early Proterozoic Koillisma layered igneous complex, NE Finland. *Geol. Surv. Finland Rep. Investig.* 61, 1–22.
- Balakrishnan, S., Hanson, G.N., Rajamani, V., 1990. Pb and Nd isotope constraints on the origin of high Mg and Tholeiitic amphibolites, Kolar Schist Belt, South India. *Contrib. Mineral. Petrol.* 107, 279–292.
- Balakrishnan, S., Rajamani, V., Hanson, G.N., 1999. U–Pb ages for zircon and titanite from the Ramagiri area, Southern India: evidence for accretionary origin of eastern Dharwar craton during Late Archean. *J. Geol.* 107, 69–86.
- Balam, V., Ramesh, S.L., Anjaniah, K.V., 1996. New trace element and REE data in thirteen GSF reference samples by ICP-MS. *Geostand. News Lett.* 20, 71–78.
- Barley, M.E., Eisenlohr, B., Groves, D.I., Perring, C.S., Vearncombe, J.R., 1989. Late Archean convergent margin tectonics and gold mineralization; a new look at the Norseman–Wiluna belt, Western Australia. *Geology* 17, 826–829.
- Barley, M.E., Krapp, B., Groves, D.I., Kerrich, R., 1998. The late Archean bonanza: metallogenic and environmental consequences of the interaction between mantle plumes, lithospheric tectonics and global cyclicity. *Precambrian Res.* 91, 65–90.
- Beeraiah, M.B., Sengupta, S., Venkataswamy, Ramachandran, T.V., 2001. Exploration for gold in sulphidic banded magnetite chert band of Nagavi-Malasamudra area, Gadag schist belt. *Geol. Surv. India Spec. Publ.* 58, 339–344.
- Bhatia, M.R., 1983. Plate tectonics and geochemical composition of sandstones. *J. Geol.* 91, 611–627.
- Bhatia, M.R., 1985. Rare earth element geochemistry of Australian Paleozoic graywackes and mudrocks: provenance and tectonic control. *Sed. Geol.* 45, 97–113.
- Bhatia, M.R., Crook, K.A.W., 1986. Trace element characteristics of greywackes and tectonic setting discrimination of sedimentary basins. *Contrib. Mineral. Petrol.* 92, 181–193.
- Bierlein, F.P., Fuller, T., Stuwe, K., Arne, D.C., Keays, R.R., 1998. Wallrock alteration associated with turbidite-hosted gold deposits. Examples from the Palaeozoic Lachlan Fold Belt in central Victoria, Australia. *Ore Geol. Rev.* 13, 345–380.
- Bierlein, F.P., Arne, D.C., McKnight, S., Lu, J., Reeves, S., Besanko, J., Marek, J., Cooke, D., 2000. Wall-rock petrology and geochemistry in alteration halos associated with mesothermal gold mineralization, Central Victoria, Australia. *Econ. Geol.* 95, 283–312.
- Bierlein, F.P., Cartwright, I., McKnight, S., 2001. The role of carbonaceous “indicator” slates in the genesis of lode gold mineralization in the Western Lachlan orogen, Victoria, Southeastern Australia. *Econ. Geol.* 96, 431–451.
- Bierlein, F.P., Christie, A.B., Smith, P.K., 2004. A comparison of orogenic gold mineralization in central Victoria (AUS), western South Island (NZ) and Nova Scotia (CAN): implications for variations in the endowment of Palaeozoic metamorphic terrains. *Ore Geol. Rev.* 25, 125–168.
- Borah, K., Rai, S.S., Gupta, S., Prakasam, K.S., Kumar, S., Sivaram, K., 2014. Preserved and modified mid-Archaean crustal blocks in Dharwar Craton: seismological evidence. *Precambrian Res.* 246, 16–34.
- Cabri, L.J., Chrysooulis, S.L., De Villiers, J.P.R., Lafamme, J.H.G., Buseck, R.R., 1989. The nature of “invisible” gold in arsenopyrite. *Can. Mineral.* 27, 353–362.
- Caddey, S.W., Bachman, R.L., Campbell, T.J., Reid, R.R., Otto, R.P., 1991. The Homestake Gold Mine, an Early Proterozoic Iron Formation-hosted Gold Deposit, Lawrence County, South Dakota. *United States Geological Survey Bulletin* 1857–J.
- Campbell, L.H., Lesher, C.M., Coad, P., Frankim, J.M., Gorton, M.P., Thurston, P.C., 1984. Rare earth mobility in alteration pipes below massive Cu–Zn-sulphide deposits. *Chem. Geol.* 45, 181–202.
- Chadwick, B., Vasudev, V.N., Hegde, G.V., 2000. The Dharwar craton, Southern India, interpreted as the result of Late Archaean oblique convergence. *Precambrian Res.* 99, 91–111.
- Chadwick, B., Vasudev, V.N., Hegde, G.V., 2003. The Chitradurga schist belt and its adjacent plutonic rocks, NW of Tungabhadra, Karnataka: a duplex in the Late Archaean convergent setting of the Dharwar craton. *J. Geol. Soc. India* 61, 645–663.
- Chalapathi Rao, N.V., Creaser, R.A., Lehmann, B., Panwar, B.K., 2013. Re–Os isotope study of Indian kimberlites and lamproites: implications for mantle source regions and cratonic evolution. *Chem. Geol.* 353, 36–47.
- Chardon, D., Peucat, J.-J., Jayananda, M., Choukroune, P., Fanning, C.M., 2002. Archean granite-greenstone tectonics at Kolar (South India): interplay of diapirism and bulk inhomogeneous contraction during magmatic juvenile accretion. *Tectonics* 21, 10–16.
- Chardon, D., Jayananda, M., Peucat, J.J., 2011. Lateral constrictional flow of hot orogenic crust: insights from the Neoproterozoic of south India, geological and geophysical implications for orogenic plateau. *Geochem. Geophys. Geosyst.* 12, Q02005.
- Clark, M.E., Archibald, N.J., Hodgson, C.J., 1986. The structural setting of the Victory Gold Mine, Kambalda, Western Australia. In: Macdonald, A.J. (Ed.), *Proceedings of Gold '86*, Toronto, pp. 243–254.
- Cox, S.F., Sun, S.-S., Etheridge, M.A., Wall, V.J., Potter, T.F., 1995. Structural and geochemical controls on the development of turbidite-hosted gold quartz vein deposits, Wattle Gully Mine, Central Victoria, Australia. *Econ. Geol.* 90, 1722–1746.
- Curtis, L.C., Radhakrishna, B.P., 1993. Gadag Gold: A Challenging Prospect. *Geological Society of India, Bangalore* (195 pp.).
- Devaraju, T.C., Viljoen, R.P., Sawkar, R.H., Sudhakar, T.L., 2009. Mafic and ultramafic magmatism and associated mineralization in the Dharwar Craton, Southern India. *J. Geol. Soc. India* 73, 73–100.
- Elder, D., Cashman, S.M., 1992. Tectonic control and fluid evolution in the Quartz Hill, California, Lode Gold Deposits. *Econ. Geol.* 87, 1795–1812.
- Giritharan, T.S., Rajamani, V., 2001. Geochemistry of ore zones in the Archean auriferous schist belts of the eastern Dharwar Craton, south India. *Proc. Indiana Acad. Sci. (Earth Planet. Sc.)* 110, 143–159.
- Gnaneshwar Rao, T., Govil, P.K., 1995. Merits of using barium as a heavy absorber in major element analysis of rock samples by X-ray fluorescence: new data on ASK-1 and ASK-2 reference samples. *Analyst* 120, 1279–1282.
- Goldfarb, R.J., Phillips, G.N., Nokleberg, W.J., 1998. Tectonic setting of synorogenic gold deposits of the Pacific Rim. *Ore Geol. Rev.* 13, 185–218.
- Goldfarb, R.J., Groves, D.I., Gardolla, S., 2001. Orogenic gold and geological time: a global synthesis. *Ore Geol. Rev.* 18, 1–75.
- Goldfarb, R.J., Baker, T., Dube, B., Groves, D.I., Hart, C.J.R., Gosselin, P., 2005. Distribution, character and genesis of gold deposits in metamorphic terrains. *Economic Geology* 100th Anniversary Volume, pp. 407–450.
- Groves, D.I., Foster, R.P., 1993. Archean lode gold deposits. In: Foster, R.P. (Ed.), *Gold Metallogeny and Exploration*. Chapman and Hall, London, pp. 63–103.
- Groves, D.I., Phillips, G.N., Ho, S.E., Houston, S.M., Standing, C.A., 1987. Craton scale distribution of Archean greenstone belt gold deposits: predictive capacity of metamorphic model. *Econ. Geol.* 82, 2045–2058.
- Groves, D.I., Goldfarb, R.J., Gebre-Mariam, M., Hagemann, S.G., Robert, F., 1998. Orogenic gold deposits: a proposed classification in the context of their crustal distribution and relationship to other gold deposit types. *Ore Geol. Rev.* 13, 7–27.
- Groves, D.I., Goldfarb, R.J., Robert, F., Hart, C.J.R., 2003. Gold deposits in metamorphic belts: overview of current understanding, outstanding problems, future research, and exploration significance. *Econ. Geol.* 98, 1–29.

- Hamilton, J.V., Hodgson, C.J., 1986. Mineralization and structure of the Kolar gold field, India. In: Macdonald, A.J. (Ed.), *Proceedings of Gold '86, Toronto*, pp. 270–283.
- Hodgson, C.J., 1993. Mesothermal lode-gold deposits. In: Kirkham, R.V., Sinclair, W.D., Thorpe, R.I., Duke, J.M. (Eds.), *Mineral Deposit Modelling*. Geological Association of Canada Special Paper 40, pp. 635–678.
- Hofstra, A.H., Cline, J.S., 2000. Characteristics and models for Carlin-type gold deposits. *Rev. Econ. Geol.* 13, 163–220.
- Huston, D.L., 2000. Gold in volcanic-hosted massive sulfide deposits: distribution, genesis and exploration. *Rev. Econ. Geol.* 13, 401–426.
- Jayananda, M., Moyen, J.F., Martin, H., Peucat, J.J., Aurvay, B., Mahabaleswar, B., 2000. Late Archaean (2550–2520) juvenile magmatism in the eastern Dharwar craton, southern India: constraints from geochronology, Nd–Sr isotopes and whole rock geochemistry. *Precambrian Res.* 99, 225–254.
- Jayananda, M., Chardon, D., Peucat, J.-J., Capdevila, R., 2006. 2.61 Ga potassic granites and crustal reworking in the western Dharwar Craton, southern India: tectonic, geochronologic and geochemical constraints. *Precambrian Res.* 150, 1–26.
- Jayananda, M., Kano, T., Peucat, J.J., Channabasappa, S., 2008. 3.35 Ga komatiite volcanism in the western Dharwar craton, southern India: constraints from Nd isotopes and whole rock geochemistry. *Precambrian Res.* 162, 160–179.
- Jayananda, M., Banerjee, M., Pant, N.C., Dasgupta, S., Kano, T., Mahesha, N., Mahabaleswar, B., 2011. 2.62 high-temperature metamorphism in the central part of Eastern Dharwar Craton: implications for late Archean tectonothermal history. *Geol. J.* 47, 213–236.
- Jayananda, M., Peucat, J.-J., Chardon, D., Krishna Rao, B., Fanning, C.M., 2012. Neoproterozoic greenstone volcanism and continental growth, Dharwar craton, southern India: constraints from SIMS U–Pb zircon geochronology and Nd isotopes. *Precambrian Res.* <http://dx.doi.org/10.1016/j.precambres.2012.05.002>.
- Jayananda, M., Peucat, J.J., Chardon, D., Krishna Rao, B., Fanning, C.M., Corfu, F., 2013. Neoproterozoic greenstone volcanism and continental growth, Dharwar Craton, southern India: constraints from SIMS U–Pb zircon geochronology and Nd isotopes. *Precambrian Res.* 227, 55–76.
- Jayananda, M., Gireesh, R.V., Sekhamo, K.-U., Miyazaki, T., 2014. Coeval felsic and mafic magmas in Neoproterozoic calc-alkaline magmatic arcs, Dharwar Craton, southern India: field and petrographic evidence from mafic and hybrid magmatic enclaves and synplutonic mafic dykes. *J. Geol. Soc. India* 84, 5–28.
- Kaila, K.L., Roy Chowdhury, K., Reddy, P.R., Krishna, V.G., Narain, Hari, Sabbotin, S.I., Sollogub, V.B., Chekunov, A.V., Kharetchko, G.E., Lazarenko, M.A., Ilehenco, T.V., 1979. Crustal structure along Kavali–Udupi profile in the Indian peninsular shield from deep seismic sounding. *J. Geol. Soc. India* 20, 307–333.
- Kerrich, R., 1993. Perspectives on genetic models for lode gold deposits. *Mineral. Deposita* 28, 362–365.
- Kerrich, R., Cassidy, K.F., 1994. Temporal relationship of lode gold mineralisation to accretion, magmatism, metamorphism and deformation–Archaean to present: a review. *Ore Geol. Rev.* 9, 263–310.
- Kerrich, R., Fryer, B.J., 1979. Archaean precious metal hydrothermal systems: Dome mine, Abitibi greenstone belt, II REE and oxygen isotope relations. *Can. J. Earth Sci.* 16, 440–458.
- Kerrich, R., Goldfarb, R.J., Groves, D.I., Garwin, S., 2000. The geodynamics of world-class gold deposits: characteristics, space-time distribution, and origins. *Rev. Econ. Geol.* 13, 501–551.
- Kerswill, J.A., 1996. Iron Formation-hosted strata-bound gold, in *Geology of Canadian Mineral Deposit Types*. DNAG-Can. 8, 367–382.
- Kolb, J., Kisters, A.F.M., Hoernes, S., Meyer, F.M., 2000. The origin of fluids and nature of fluid–rock interaction in mid-crustal auriferous mylonites of the Renco mine, southern Zimbabwe. *Mineral. Deposita* 35, 109–125.
- Kontak, D.J., Smith, P.K., Kerrich, R., Williams, P.F., 1990. Integrated model for Meguma Group lode gold deposits, Nova Scotia, Canada. *Geology* 18, 238–242.
- Krogstad, E.J., Hanson, G.N., Rajamani, V., 1991. U–pb ages of zircon and sphene for two gneiss terranes adjacent to the Kolar Schist belt, south India: evidence for separate crustal evolution histories. *J. Geol.* 99, 801–816.
- Large, R.R., Bull, S.W., Maslennikov, V., 2011. A carbonaceous sedimentary source-rock model for Carlin-type and orogenic gold deposits. *Econ. Geol. Bull. Soc. Econ. Geol.* 106, 331–358.
- Law, J.D.M., Phillips, G.N., 2005. Hydrothermal replacement model for Witwatersrand gold. *Economic Geology 100th Anniversary Volume*, pp. 799–812.
- Lu, H.-Z., Wang, Z., Chen, W., Wu, X., Hu, R., 2005. Turbidite hosted bedding parallel gold quartz veins in SE Guizhou, China. *Acta Geol.* 1, 22–26.
- Maclaren, J.M., 1906. Notes on some auriferous tracts in Southern India. *Geol. Surv. India Rec.* 34, 96–131.
- Malapur, M.A., Manjunatha, S., Chandan Kumar, B., Ugarkar, A.G., 2012. Ore fluids associated with the metasediment hosted Central Auriferous zones of Gadag Gold Field, Karnataka. *Int. J. Earth Sci. Eng.* 5, 1545–1551.
- Manikyamba, C., Kerrich, R., 2011. Geochemistry of alkaline basalts and associated high-Mg basalts from the 2.7 Ga Penakcherla Terrane, Dharwar Craton, India: an Archaean depleted mantle–OIB array. *Precambrian Res.* 188, 104–122.
- Manikyamba, C., Naqvi, S.M., Ram Mohan, M., Gnaneshwar Rao, T., 2004. Gold mineralization and alteration of Penakcherla schist belt, India, constraints on Archaean subduction and fluid processes. *Ore Geol. Rev.* 24, 199–227.
- Manikyamba, C., Kerrich, R., Khanna, T.C., Krishna, A.K., Satyanarayanan, M., 2008. Geochemical systematics of komatiite–tholeiite and adakite–arc basalt associations: the role of a mantle plume and convergent margin in formation of the Sandur Superterrane, Dharwar Craton, India. *Lithos* 16, 155–172.
- Manikyamba, C., Saha, Abhishek, Santosh, M., Ganguly, Sohini, Rajanikanta Singh, M., Subba Rao, D.V., Lingadevaru, M., 2014. Neoproterozoic felsic volcanic rocks from the Shimoga greenstone belt, Dharwar Craton, India: geochemical fingerprints of crustal growth at an active continental margin. *Precambrian Res.* 252, 1–21.
- McCuaig, T.C., Kerrich, R., 1998. P–T–t deformation–fluid characteristics of lode gold deposits: evidences of lode gold deposits: evidence from alteration systematic. *Ore Geol. Rev.* 12, 381–453.
- McLennan, S.M., Taylor, S.R., 1991. Sedimentary rocks and crustal evolution: tectonic setting and secular trends. *J. Geol.* 99, 1–21.
- McLennan, S.M., McCulloch, M.T., Taylor, S.R., Maynard, J.B., 1990. Geochemical and Nd–Sr isotopic composition of deep-sea turbidites: crustal evolution and plate tectonic associations. *Geochim. Cosmochim. Acta* 54, 2015–2050.
- Mishra, B., Pal, N., 2008. Metamorphism, fluid flux and fluid evolution relative to gold mineralization in the Hutti–Maski greenstone belt, Eastern Dharwar Craton, India. *Econ. Geol.* 103, 801–827.
- Mueller, A.G., Groves, D.I., 1991. The classification of western Australian greenstone hosted gold deposits according to wall rock alteration mineral assemblages. *Ore Geol. Rev.* 6, 291–331.
- Naqvi, S.M., Rogers, J.J.W., 1987. *Precambrian Geology of India*. Oxford University Press, New York (223 pp.).
- Narayanawamy, S., Ahmed, M., 1963. *Geology of Gadag gold field, Dharwar district, Mysore State*. *Geol. Soc. India Mem.* 1, 107–116.
- Nutman, A.P., Chadwick, B., Krishna Rao, B., Vasudev, V.N., 1996. SHRIMP U–Pb zircon ages of acid volcanic rocks in the Chitradurga and Sandur groups and granites adjacent to Sandur schist belt. *J. Geol. Soc. India* 47, 153–164.
- Pan, Y., Fleet, M.E., 1990. Halogen-rich allanite from the white River gold occurrence, Hemlo area, Ontario. *Can. Mineral.* 28, 67–75.
- Pan, Y., Fleet, M.E., Barnet, R.L., 1994. Rare earth mineralogy and geochemistry at the Mattagamy volcanogenic massive sulphide deposit, Quebec. *Can. Mineral.* 32, 133–147.
- Peucat, J.J., Mahabaleswar, B., Jayananda, M., 1993. Age of younger tonalitic magmatism and granulitic metamorphism in the South Indian transition zone (Krishnagiri area): comparison with older peninsular gneisses from the Gorur–Hassan area. *J. Metamorph. Geol.* 11, 879–888.
- Peucat, J.J., Jayananda, M., Chardon, D., Capdevila, R., Fanning, C.M., Paquette, J.-L., 2013. The lower crust of the Dharwar Craton, south India: patchwork of Archean granulitic domains. *Precambrian Res.* 227, 4–28.
- Phillips, G.N., Powell, R., 2009. Formation of gold deposits: review and evaluation of the continuum model. *Earth-Sci. Rev.* 94, 1–21.
- Pili, E., Ricard, Y., Lardeaux, J.M., Sheppard, S.M.F., 1997. Sheppard lithospheric shear zones and mantle–crust connections. *Tectonophysics* 280, 15–29.
- Poulsen, K.H., Rober, F., Dube, B., 2000. Geological classification of Canadian gold deposits. *Geol. Surv. Can. Bull.* 540 (106 pp.).
- Radhakrishna, B.P., Curtis, L.C., 1999. *Gold in India*. Geological Society of India, Bangalore (307 pp.).
- Radhakrishna, B.P., Vaidyanathan, R., 1997. *Geology of Karnataka*. Geological Society of India, Bangalore (353 pp.).
- Ram Mohan, M., Sarma, S.D., Neal, J.M., Fletcher, I.R., Wilde, S.A., Siddiqui, M.A., Rasmussen, B., Krapez, B., Gregory, J., Kamo, S.L., 2014. SHRIMP zircon and titanite U–Pb ages, Lu–Hf isotope signatures and geochemical constraints for ~2.56 Ga granitic magma in western Dharwar Craton, southern India: evidence for short-lived Neoproterozoic episodic crustal growth? *Precambrian Res.* 243, 197–220.
- Ramachandran, T.V., Beeraiah, M.B., Sengupta, S., 2001. Exploration for Auriferous Ore Zones in Gadag Schist Belt, Karnataka: Some Aspects of Mineral Development in India. *Geological Society of India and Department of Geology, Andhra University*, pp. 53–66.
- Ramadass, G., Ramaprasad Rao, I.B., Srinivasulu, N., Himabindu, D., 2003. Density studies in the Dharwar Craton along the Jaelcharla–Goa Subtransect. *J. Geol. Soc. India* 61, 439–448.
- Ramesh, S.L., Sunder Raju, P.V., Anjaiah, K.V., Gnaaneswar Rao, T., Dasaram, B., Nirmal Charan, S., Subba Rao, D.V., Sarma, D.S., Ram Mohan, M., Balaram, V., 2001. Determination of gold in rocks, ores and other geological materials by atomic absorption techniques. *At. Spectrosc.* 22, 263–269.
- Rao, P.S., Reddy, U.S., 1985. *Geology of gold deposits of India*. United Nations Inter Regional Seminar Volume on Gold Exploration and Development, Bangalore, pp. 21–32.
- Robert, F., Poulsen, K.H., Cassidy, K.F., Hodgson, C.J., 2005. Gold metallogeny of the Superior and Yilgarn Cratons. *Economic Geology 100th Anniversary Volume*, pp. 1001–1034.
- Robert, F., Brommecker, R., Bourne, B.T., Dobak, P.J., McEwan, C.J., Rowe, R.R., Zhou, X., 2007. Models and exploration methods for major gold deposit types. In: Milkereit, B. (Ed.), *Ore Deposits and Exploration Technology, Proceedings of Fifth Decennial International Conference on Mineral Exploration*, pp. 691–711.
- Roedder, E., 1984. Fluid inclusions. *Mineral. Soc. Am. Rev. Mineral.* 12, 644.
- Rollinson, H.R., Windley, B.F., Ramakrishnan, M., 1981. Contrasting high and intermediate pressures of metamorphism in the Archaean Sargur schists of southern India. *Contrib. Mineral. Petrol.* 76, 420–429.
- Roser, B.P., Korsch, R.J., 1986. Determination of tectonic setting of sandstone–mudstone suites using SiO₂ content and K₂O/Na₂O ratio. *J. Geol.* 94, 635–650.
- Santosh, M., 1993. Role of mantle carbon in Archaean gold genesis in south India: evidence from carbon isotopic composition of fluid inclusions. *J. Geol. Soc. India* 40, 127–134.
- Sarang, S., Srinivasan, R., Balaram, V., 2013. REE geochemistry of auriferous quartz carbonate veins of Neoproterozoic Ajjanahalli gold deposit, Chitradurga schist belt, Dharwar Craton, India. *Geosci. Front.* 4, 231–239.
- Sarma, D.S., Fletcher, I.R., Rasmussen, B., Mc Naughton, N.J., Ram Mohan, M., Groves, D.I., 2011. Archaean gold mineralization synchronous with late cratonization of the western Dharwar Craton, India: and xenotime in gold deposits. *Mineral. Deposita* 46, 273–288.
- Sarma, D.S., McNaughton, N.J., Belusova, E., Ram Mohan, M., Fletcher, I.R., 2012. Detrital zircon U–Pb ages and Hf-isotope systematics from the Gadag greenstone belt: Archean crustal growth in the western Dharwar Craton, India. *Gondwana Res.* 22, 843–854.

- Sawkar, R.H., Hussain, S.M., Naqvi, S.M., 1995. Gold mineralization and exploration in the sulphide BIF's Chitradurga schist belt, Karnataka—possibility of new workable gold deposits. *J. Geol. Soc. India* 46, 91–94.
- Sawkar, R.H., Baldota, R., Suresh, S.R., Sastri, P.T., Kulgeri, A.S., Sarma, D.S., Subba Rao, D.V., Nirmalcharan, S., Naqvi, S.M., 1999. Exploration, mine development and pilot plant operation at Gadag Gold Field, Karnataka, India. *J. Geol. Soc. India* 54, 322–326.
- Sengupta, S., Roy, A., 2012. Tectonic amalgamation of crustal blocks along Gadag–Mandya shear zone in Dharwar Craton of southern India. *J. Geol. Soc. India* 80, 75–88.
- Sibson, R.H., 1990. Faulting and fluid flow. *Mineral. Assoc. Can. Short Course* 18, 93–132.
- Sillitoe, R.H., Bonham, H.F., 1990. Sediment-hosted gold deposits, distal products of magmatic-hydrothermal systems. *Geology* 18, 157–161.
- Sillitoe, R.H., Thompson, J.F.H., 1998. Intrusion-related vein gold deposits – types, tectono-magmatic setting and difficulties of distinction from orogenic gold deposits. *Resour. Geol.* 48, 237–250.
- Swami Nath, J., Ramakrishnan, M., Viswanatha, M.N., 1976. Dharwar stratigraphic model and Karnataka craton evolution. *Rec. Geol. Surv. India* 107, 149–175.
- Swami Nath, J., Ramakrishnan, M., 1981. Present classification and correlation. In: Swaminath, J., Ramakrishnan, M. (Eds.), *Early Precambrian Supracrustals of Southern Karnataka*. Geological Survey of India Memoir 112, pp. 23–38.
- Taylor, S.R., McLennan, S.M., 1985. *The Continental Crust: Its Composition and Evolution*. Blackwell, London (312 pp.).
- Tomilenko, A., Gibsher, N., Dublyansky, Y., Dallai, L., 2010. Geochemical and isotopic properties of fluids from gold-bearing and barren quartz veins of the Sovetskoye gold deposits (Siberia, Russia). *Econ. Geol.* 105, 375–394.
- Tomkins, A.G., 2014. On the source of orogenic gold. *Geology* 41, 1255–1256.
- Ugarkar, A.G., 1998. Implications of retrograde metamorphism for gold mineralization in the greenstone belts of northern Dharwar Craton, Karnataka, India. *Gondwana Res.* 1, 215–219.
- Ugarkar, A.G., Deshpande, M.P., 1999. Lithology and gold mineralization of Gadag gold field, Dharwar craton – evidences for epigenesis of gold in diversified host rocks. *Indian Mineral.* 37–52.
- Ugarkar, A.G., Natikar, R.D., 2011. Rare earth element behavior during hydrothermal alteration in the western auriferous zone of Gadag gold field, Karnataka. *Indian Mineral.* 45, 265–273.
- Ugarkar, A.G., Nyamati, R.C., 2002. Geochemical characteristics of clastic metasediments of Gadag Gold field, southern India: implications for provenance and tectonic setting. *Gondwana Res.* 5, 245–255.
- Ugarkar, A.G., Tenginkai, S.G., 1988. Gold-quartz-sulphide reefs of Mangalur, Gulbarga District, Karnataka. *Curr. Sci.* 57, 143–145.
- Ugarkar, A.G., Devaraju, T.C., Halkoaho, T.A.A., 1994. Invisible gold in arsenopyrites of the auriferous zones of the Gadag gold field, Karnataka. *Curr. Sci.* 67, 605–606.
- Ugarkar, A.G., Panaskar, D.B., Ranganath Gowda, G., 2000. Geochemistry, petrogenesis and tectonic setting of metavolcanics and their implications for gold mineralization in Gadag gold field, southern India. *Gondwana Res.* 3, 371–384.
- Ugarkar, A.G., Devaraju, T.C., Alapieti, T.T., Halkoaho, T.A.A., 2007. Occurrence of monazite in the auriferous zones of Gadag gold field, Karnataka. *Curr. Sci.* 67, 1763–1767.
- Ugarkar, A.G., Solankar, S.N., Vasudev, V.N., 2013. Geology and geochemistry of Archaean felsic metavolcanic rocks of the eastern part of the Kolar greenstone belt, Dharwar Craton, India: implications for their petrogenesis and geodynamic setting. *J. Geol. Soc. India* 81, 192–202.
- Vasudev, V.N., Ranganathan, N., Srikantamurthy, D., 1994. Lithostratigraphic distribution of gold ore resources in Karnataka: in Geo-Karnataka. In: Ravindra, B.M., Ranganathan, N. (Eds.), *Mysore Geological Department Centenary volume*, pp. 182–192.
- Wyman, D., Kerrich, R., 1988. Alkaline magmatism, major structures and gold deposits: implications for greenstone belt gold metallogeny. *Econ. Geol.* 83, 451–456.
- Wyman, D.A., Kerrich, R., Groves, D.I., 1999. Lode gold deposits and Archaean mantle plume-island arc interaction, Abitibi subprovince, Canada. *J. Geol.* 107, 715–725.
- Xue, Y., Campbell, I.H., Ireland, T.R., Holden, P., Armstrong, R., 2013. No mass-independent sulfur isotope fractionation in auriferous fluids supports a magmatic origin for Archean gold deposits. *Geology* 41, 791–794.
- Yakubchuk, A., Cole, A., Seltmann, R., Shatov, V., 2002. Tectonic setting, characteristics, and regional exploration criteria for gold mineralization in the Altaid orogenic collage – the Tien Shan province as a key example. *Soc. Econ. Geol. Spec. Publ.* 9, 177–201.
- Zhou, T., Goldfarb, R.J., Phillips, G.N., 2002. Tectonics and distribution of gold deposits in China: an overview. *Mineral. Deposita* 37, 249–282.